

AD-A198 642

DTIC FILE COPY

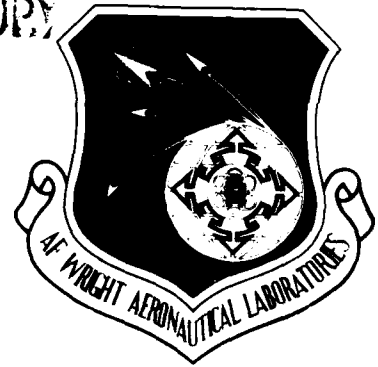
1

AFWAL-TR-88-3032

AUTOMATED FATIGUE CRACK GROWTH MEASUREMENT

Ted E. Kirchner
John McCoy

Foster-Miller, Inc.
350 Second Avenue
Waltham, MA 02254



May 1988

Final Report for Period July 1987 - January 1988

Approved for Public Release; Distribution is Unlimited

DTIC
ELECTE
AUG 10 1988
S H D

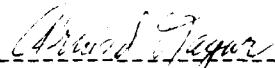
FLIGHT DYNAMICS LABORATORY
AIR FORCE WRIGHT AERONAUTICAL LABORATORIES
AIR FORCE SYSTEMS COMMAND
WRIGHT-PATTERSON AIR FORCE BASE, OHIO 45433-6553

NOTICE

WHEN GOVERNMENT DRAWINGS, SPECIFICATIONS, OR OTHER DATA ARE USED FOR ANY PURPOSE OTHER THAN IN CONNECTION WITH A DEFINITELY GOVERNMENT-RELATED PROCUREMENT, THE UNITED STATES GOVERNMENT INCURS NO RESPONSIBILITY OR ANY OBLIGATION WHATSOEVER. THE FACT THAT THE GOVERNMENT MAY HAVE FORMULATED OR IN ANY WAY SUPPLIED THE SAID DRAWINGS, SPECIFICATIONS, OR OTHER DATA, IS NOT TO BE REGARDED BY IMPLICATION, OR OTHERWISE IN ANY MANNER CONSTRUED, AS LICENSING THE HOLDER, OR ANY OTHER PERSON OR CORPORATION; OR AS CONVEYING ANY RIGHTS OR PERMISSION TO MANUFACTURE, USE, OR SELL ANY PATENTED INVENTION THAT MAY IN ANY WAY BE RELATED THERETO.

THIS REPORT HAS BEEN REVIEWED BY THE OFFICE OF PUBLIC AFFAIRS (ASD/CPA) AND IS RELEASABLE TO THE NATIONAL TECHNICAL INFORMATION SERVICE (NTIS). AT NTIS, IT WILL BE AVAILABLE TO THE GENERAL PUBLIC, INCLUDING FOREIGN NATIONS.

THIS TECHNICAL REPORT HAS BEEN REVIEWED AND IS APPROVED FOR PUBLICATION.

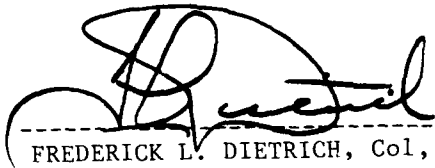


ARVIND NAGAR, Project Engr
Fatigue, Fracture & Reliability Gp
Structural Integrity Branch



DONALD B. PAUL, Actg Chief
Structural Integrity Branch
Structures Division

FOR THE COMMANDER



FREDERICK L. DIETRICH, Col, USAF
Chief, Structures Division

IF YOUR ADDRESS HAS CHANGED, IF YOU WISH TO BE REMOVED FROM OUR MAILING LIST, OR IF THE ADDRESSEE IS NO LONGER EMPLOYED BY YOUR ORGANIZATION PLEASE NOTIFY AFWAL/FIBEC, WRIGHT-PATTERSON AFB, OH 45433-6553 TO HELP US MAINTAIN A CURRENT MAILING LIST.

COPIES OF THIS REPORT SHOULD NOT BE RETURNED UNLESS RETURN IS REQUIRED BY SECURITY CONSIDERATIONS, CONTRACTUAL OBLIGATIONS, OR NOTICE ON A SPECIFIC DOCUMENT.

REPORT DOCUMENTATION PAGE

1a. REPORT SECURITY CLASSIFICATION Unclassified		1b. RESTRICTIVE MARKINGS	
2a. SECURITY CLASSIFICATION AUTHORITY		3. DISTRIBUTION / AVAILABILITY OF REPORT Approved for Public Release; Distribution is Unlimited	
2b. DECLASSIFICATION / DOWNGRADING SCHEDULE			
4. PERFORMING ORGANIZATION REPORT NUMBER(S) AFW-8767		5. MONITORING ORGANIZATION REPORT NUMBER(S) AFWAL TR-88-3032	
6a. NAME OF PERFORMING ORGANIZATION Foster-Miller, Inc.	6b. OFFICE SYMBOL (if applicable)	7a. NAME OF MONITORING ORGANIZATION Flight Dynamics Laboratory (AFWAL/FIBEC) AF Wright Aeronautical Laboratories	
6c. ADDRESS (City, State, and ZIP Code) 350 Second Avenue Waltham, MA 02254		7b. ADDRESS (City, State, and ZIP Code) WPAFB, OH 45433-6553	
8a. NAME OF FUNDING / SPONSORING ORGANIZATION DoD SBIR Program Office	8b. OFFICE SYMBOL (if applicable)	9. PROCUREMENT INSTRUMENT IDENTIFICATION NUMBER F33615-87-C-3240	
8c. ADDRESS (City, State, and ZIP Code) Washington DC 20301		10. SOURCE OF FUNDING NUMBERS	
		PROGRAM ELEMENT NO. 65502F	PROJECT NO. 3005
		TASK NO. 30	WORK UNIT ACCESSION NO. 90
11. TITLE (Include Security Classification) Automated Fatigue Crack Growth Measurement			
12. PERSONAL AUTHOR(S) Ted E. Kirchner, John McCoy			
13a. TYPE OF REPORT Final	13b. TIME COVERED FROM 7/28/87 TO 1/28/88	14. DATE OF REPORT (Year, Month, Day) 1988 July	15. PAGE COUNT 69
16. SUPPLEMENTARY NOTATION "Export Control Restrictions Apply" This is a Small Business Innovation Research Program Report			
17. COSATI CODES		18. SUBJECT TERMS (Continue on reverse if necessary and identify by block number)	
FIELD	GROUP	SUB-GROUP	
19. ABSTRACT (Continue on reverse if necessary and identify by block number) Fatigue testing is a key element in the development of aircraft and engines. The higher performance temperatures of both airframe and engines of future aircraft makes precise high temperature fatigue testing vital. The goal of this program is to develop a new tool that will automate this test and provide fatigue crack measurement to a precision of 0.001 in. at varying temperatures up to 2000°F and likely higher. In the Phase I program reported here we have experimentally shown the feasibility of two different approaches using laser and γ-ray technology. We have recommended that the laser approach be selected for hardware development. A system design of a laser automated fatigue crack measurement instrument is presented and will form the basis of a sound Phase II program.			
20. DISTRIBUTION / AVAILABILITY OF ABSTRACT <input checked="" type="checkbox"/> UNCLASSIFIED/UNLIMITED <input type="checkbox"/> SAME AS RPT. <input type="checkbox"/> DTIC USERS		21. ABSTRACT SECURITY CLASSIFICATION Unclassified	
22a. NAME OF RESPONSIBLE INDIVIDUAL Dr. Arvind Nagar		22b. TELEPHONE (Include Area Code) (513) 255-6104	22c. OFFICE SYMBOL AFWAL/FIBEC

TABLE OF CONTENTS

<u>Section</u>	<u>Page</u>
1. INTRODUCTION.....	1-1
2. FATIGUE CRACK MEASUREMENT APPROACHES.....	2-1
2.1 Argon Laser Approach.....	2-3
2.2 X-Ray Approach.....	2-6
3. PROGRAM PLAN.....	3-1
4. EXPERIMENTS AND RESULTS.....	4-1
4.1 Laser Experiments.....	4-1
4.1.1 Room Temperature Tests.....	4-1
4.1.2 Hot Tests.....	4-7
4.1.3 Results.....	4-13
4.2 X-Ray Experiments.....	4-15
4.2.1 X-Ray Testing.....	4-15
4.2.2 Results.....	4-15
5. EXPERIMENT CONCLUSIONS AND RECOMMENDATIONS.....	5-1
5.1 Laser Experiment.....	5-1
5.2 X-Ray Experiment.....	5-1
5.3 Sensor Selection and Recommendations.....	5-1
6. SYSTEM DESIGN.....	6-1
6.1 System Description.....	6-3
6.2 Vision System Description.....	6-5
6.3 Mobile Sensor System Description.....	6-8

For	
<input checked="checked" type="checkbox"/>	
<input type="checkbox"/>	
<input type="checkbox"/>	
on	
n,	
ty Codes	
and/or	
Dist	Special
A-1	

TABLE OF CONTENTS (Continued)

<u>Section</u>		<u>Page</u>
6.4	Simultaneous Crack Measurement from Both Sides.....	6-11
6.5	Higher Temperature Measurement Capability....	6-12
APPENDIX A	LASER EXPERIMENT DATA.....	A-1
APPENDIX B	X-RAY EXPERIMENT DATA.....	B-1

LIST OF ILLUSTRATIONS

<u>Figure</u>		<u>Page</u>
1-1	Automatic Fatigue Crack Growth Measurement Performance Requirements.....	1-1
2-1	Laser Illumination Combined with Narrow-Band Interference Filter Discriminates Against the Thermal Self-Radiation at High Temperatures (3).	2-4
2-2	Argon Laser Sensor Systems.....	2-5
2-3	X-Ray Sensor System.....	2-7
3-1	Program Plan.....	3-1
4-1	Inconel Specimen.....	4-3
4-2	Laser Room Temperature Test Configuration.....	4-3
4-3	Specimen Illuminated with HeNe Laser Beam.....	4-7
4-4	Stainless Steel Specimen with Thermocouple Probe.....	4-9
4-5	Self-Radiation only at 2,000°F.....	
4-11		
4-6	Specimen at 2,000°F Illuminated by Argon-Ion Laser.....	4-11
4-7	Narrow Band Pass Filter Characteristics, Centered on Argon-Ion Wavelength.....	4-13
4-8	Specimen at 2,000°F Illuminated by Argon Ion Laser Viewed Through Narrow Band Pass Filter....	4-13
4-9	X-Ray Test Setup.....	4-15
4-10	X-Ray Testing.....	4-17
4-11	Radiograph of Inconel Test Specimen.....	4-19
6-1	Proposed System Concept.....	6-1
6-2	Proposed Linesian Laser System	6-2
6-3	System Design Concept.....	6-3

LIST OF ILLUSTRATIONS (Continued)

<u>Figure</u>		<u>Page</u>
6-4	Crack Measurement System Mobile Sensor Subsystem Configuration.....	6-6
6-5	Typical Foxboro/Octek Machine Vision Equipment in NEMA Enclosures.....	6-8
6-6	Argon-Ion Laser.....	6-9

LIST OF TABLES

<u>Table</u>		<u>Page</u>
2-1	Summary of Measurement Methods.....	2-2
4-1	Film Exposure Conditions.....	4-16
4-2	Laser Experiment Data.....	4-19
4-3	X-Ray Experiment Data.....	4-20
6-1	Performance Requirements.....	6-4

1. INTRODUCTION AND SUMMARY

The application of fracture mechanics to fracture toughness and fatigue crack propagation studies is primarily dependent upon the crack length. Particularly in fatigue crack growth rate testing, where crack growth rates are related to the stress intensity range, crack length determination has long been recognized as a source of error (1).

Precise crack length determination is, then, the goal of this program. Precision was defined as 0.001 in. and furthermore this measurement should be made in real-time during fatigue loading and in varying temperatures up to 2000°F. A summary of these and other performance requirements is shown in Figure 1-1.

The key to making this measurement to the required precision in the working environment is the crack sensor. Two sensor technologies were recognized by Foster-Miller to have the potential to meet all of these

SPECIMEN:	
• MATERIAL MIN:	ALUMINUM, 0.050 IN. THICK
• MAX:	INCONEL 7-18, 0.5 IN. THICK
• CRACK RESOLUTION:	0.001 IN.
• CRACK TRACKING SPEED:	0.030 IN. PER SECOND
• TEMPERATURE RANGE:	-50°F TO 2,000°F
TEST MACHINE: (MTS, 2 POST, 100 KP FRAME SIZE)	
• TEST FREQUENCY:	0 to 50 HZ
• OVEN WINDOW:	4 IN. x 1.8 IN. QUARTZ
ENVIRONMENT:	
• AIR CONDITIONED LABORATORY	
• CLEARANCE:	30 IN. BEHIND, 36 IN. FROM

Figure 1-1. Automatic Fatigue Crack Growth Measurement
Performance Requirements

requirements and to have the capacity to be configured into a completely automated system. These technologies were based on laser and x-ray detection; a discussion of the approaches taken appears in Section 2 of this report and the plan followed to demonstrate, evaluate and select the better approach is in Section 3.

Demonstration was based on well-defined experiments. There is no doubt that cracks can be imaged with laser or x-ray illumination. The concerns were different for the two sensors:

- Could the laser camera see a crack in a specimen that was self-illuminating at 2000^oF?
- Could the x-ray camera see a crack in a specimen that could be at large angles to the x-ray flux?

The experiments that answered these questions are described in detail and the results presented in Section 4.

The experiments showed that both the laser and x-ray approaches were viable. The selection then centered on performance margins and system implementation considerations. The laser approach was selected for implementation. This selection, the experiment conclusions and our recommendations are all presented and discussed in Section 5.

A system design to implement an automated laser crack measurement approach is presented in Section 6. Along with the design is a discussion of the implications of extending the design to the simultaneous measurement of a crack from both sides of the specimen and the extension of the crack measurement temperature environment to 4,000^oF and 5,000^oF.

2. FATIGUE CRACK MEASUREMENT APPROACHES

Various methods for the determination of crack length have been developed and used with varying degrees of success, depending upon the particular circumstances. We have reviewed these methods with respect to the Air Force requirements and concluded that manual microscopic examination remains the best. Table 2-1 is a summary from that review which compares the known fatigue crack measurement methods.

Apart from the optical technique, all procedures of potential interest to the USAF have one common disadvantage: crack size is measured indirectly by measuring a quantity (compliance, strain, potential drop) that depends upon crack size. Since the relation between the measured quantity and crack size is often not known accurately, calibrations are usually necessary. Different structural geometries and crack geometries require separate calibration. All measured quantities are affected by either crack tip plasticity or crack closure (2) or both. This may invalidate or degrade the calibration for flight-by-flight testing. All methods are integrators: what is actually measured (be it indirectly) is cracked area and not crack length. For through cracks, therefore, an average (through the thickness) crack length is obtained. All methods can be easily used in automated testing.

Direct measurement of crack size by the optical technique does not have most of these disadvantages, although it measures only the surface evidence of the crack. In the proposed approaches yet to be discussed, this limitation can be readily overcome, or, in the case of the x-ray approach, does not exist.

Automation of optical measurement requires Image Array Processors (IAP) which digitize the video image and allow rapid computerized analysis of that image. Image enhancement by both hardware (illumination, magnification, etc.) and software can be used to define the crack image. Recent advances in digital image processing technology relegate this portion of the problem to a straightforward engineering solution which is discussed at length in Section 6.

Table 2-1. Summary of Measurement Methods

Method	Accuracy	Is Accuracy Affected by Plasticity and Crack Closure?	Is Calibration Direct and Easy?	Calibration Uniqueness	Versatility for Different Specimens and Crack Types	Is Standard Hardware Available for Stable Signals?	Reliability	Is Automation Easy?	Is the System Safe	Is the System Expensive?
1. Optical (Manual)	Good	No	Yes	Good	Good	Yes	Good	-	Safe	No
2. Optical (Image processor)	Good	No	Yes	Good	Good	Yes	Good	Yes	Safe	?
3. Compliance and COD	Poor	Yes	No	Fair	Poor	Yes	Fair	Yes	Safe	No
4. Backface Strain	Good/Fair	Yes	No	Fair	Poor	?	Fair	Yes	Safe	No
5. Direct Current Potential Drop	Fair	Yes	No	Fair	Poor	?	Fair	Yes	Safe	No
6. Alternating Current Potential Drop	Fair	Yes	No	Fair	Poor	?	Fair	Yes	Safe	No
7. Ultrasonic	Poor	Yes	No	Poor	Poor	No	Poor	No	Safe	Yes
8. Acoustic Emission	Poor	Yes	No	Poor	Poor	No	Poor	No	Safe	Yes
9. Eddy Current Travelling Probe	Fair	Yes	No	Fair	Poor	No	Fair	No	Safe	Yes
10. Exoelectron Emission	Good	?	No	?	Good	No	?	?	?	?

Whereas the digital imaging approach has many advantages for quantifying cracks at room temperature, samples at elevated temperatures up to $2,000^{\circ}\text{F}$ present two severe problems.

- First, the thermal radiation from such samples is intense, spectrally broadband and geometrically isotropic. It may overwhelm any external illumination as supplied in room temperature systems to enhance crack contrast by careful control of illumination angle. On the other hand, if digital imaging were to be applied using only the thermal self-illumination, the crack contrast would be low, even taking into account the extra brightness that may be found inside the crack itself due to black-body effects. In short, the important ability to adjust system illumination would be lost
- Second, the digital imaging camera itself might not withstand the hot environment if placed within a meter of such a furnace. As a rule of thumb, the camera should not be placed in an environment thermally uncomfortable for a human observer.

If we believe that direct measurement is best, then we must retain this approach and find ways to overcome the "noise" generated by the $2,000^{\circ}\text{F}$ environment. Two possibilities present themselves. One would operate in an extremely narrow bandwidth in the visible light range by using a laser source and filtering techniques. The other approach would operate well above the visible light spectrum at x-ray energies and, therefore, would be immune to the thermal radiation.

2.1 Argon Laser Approach

In this approach we propose an active laser illumination scheme in combination with narrow-band optical filters to "cut through" the unwanted thermal radiation.

The principle can be understood by reference to the irradiance spectrum illustrated schematically in Figure 2-1. The left graph shows the black-body radiation emitted by the surface of an object at $1,000^{\circ}\text{K}$ ($1,341^{\circ}\text{F}$). At

the peak emittance wavelength of $3\mu\text{m}$, approximately $200\text{ mW/cm}^2\mu\text{m}^{-1}$ is present. From the black-body law $P=\sigma T^4$, the total optical and infrared power radiated is about 2W/cm^2 .

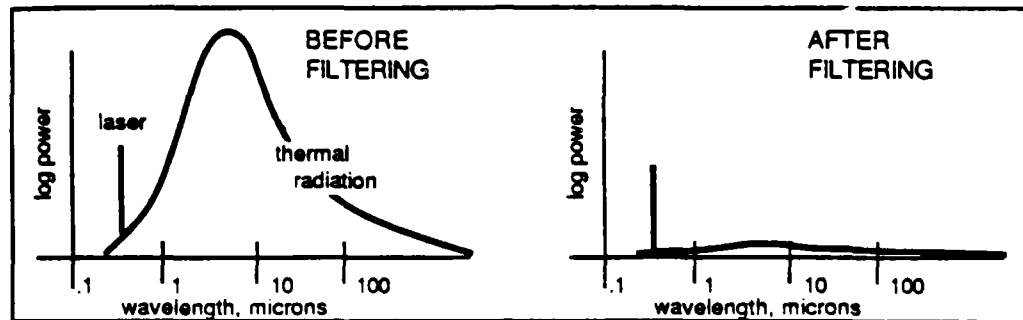


Figure 2-1. Laser Illumination Combined with Narrow-band Interference Filter Discriminates Against the Thermal Self-Radiation at High Temperatures (3)

Also shown in the left graph is a spike due to actively illuminating the sample with blue-green radiation at $0.488\mu\text{m}$ from an argon ion laser. A commercially available laser with 50 mW output power at this wavelength will illuminate the sample through a system of beam defining lenses and collimators at a level of approximately 5 mW/cm^2 . The laser illumination "signal" is present in a much larger "noise" background of thermal radiation; to the naked eye, the laser signal may be invisible against the bright background.

In Figure 2-2, we show the sensor placed at a comfortable distance from the furnace; it detects the scattered argon laser radiation from the crack through a small telescope with a defined field of view, such as a Questar. The telescope objective is covered with a long-wavelength rejection filter, available in large apertures with high reflectance (95 percent) at all wavelengths above approximately $0.7\mu\text{m}$. This protects the telescope and the video camera sensor from excessive heat and performs a first stage of optical filtering. A narrow-band interference filter is placed between the telescope and the sensor itself. This filter will have a pass-band of approximately $0.005\mu\text{m}$ centered on the argon laser line and is

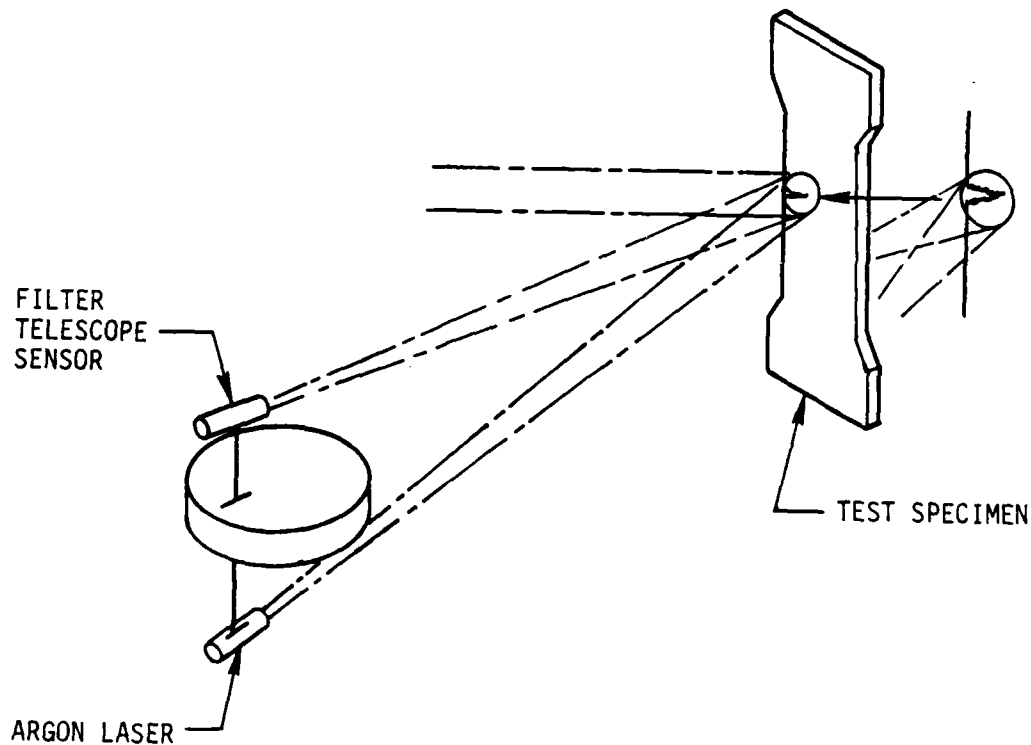


Figure 2-2. Argon Laser Sensor System

commercially available in apertures up to 5 cm. Such filters pass up to 50 percent of the peak wavelength and less than 10^{-4} of the light outside the pass-band (4).

The right graph of Figure 2-1 shows the spectral illumination as seen by the sensor after these two stages of filtering. The sample's black-body radiation has been almost entirely rejected, except for two contributions: the very small portion which passes the narrow-band filter in the pass-band

around $0.488 \mu\text{m}$, predicted from the black-body distribution law to be about $5 \times 10^{-7} \text{ mW/cm}^2$, and the remaining visible thermal radiation entering outside the pass-band, estimated to be $5 \times 10^{-3} \text{ mW/cm}^2$. The detection now takes place using effectively only the laser illumination with a signal to noise ratio of about 1,000:1 or 30 dB over the thermal background.

2.2 X-Ray Approach

In this approach, it is essential to have access from both sides of the specimen, as we will essentially be monitoring the x-ray attenuation of the specimen. As a fatigue crack begins to open, this x-ray attenuation will change significantly and is totally unaffected by all the other variables in the system.

In Figure 2-3 we show the x-ray source, in this configuration a standard 160 kV generator (such as a Magnaflux CMA1G) and an x-ray collimator to confine the x-ray beam to cover the maximum extent that a fatigue crack may wander. The x-ray detector will be stationary on the other side of the chamber using a plastic scintillator (such as NE101) slightly wider than the widest expected specimen. The scintillator converts the x-ray image to visible light which is viewed by a video camera. From here the data processing is identical to the laser approach.

The main advantage of the x-ray measurement approach is in its complete immunity from any thermal noise measurements (which may contribute to background in the visible wavelength detection band), and its (inferred) ability to measure an average position over the entire front of the crack advance. This later advantage could be significant as it would require the laser approach to incorporate two distinct detection systems viewing the test specimens from opposite sides to approximate the x-ray data from a single detector system.

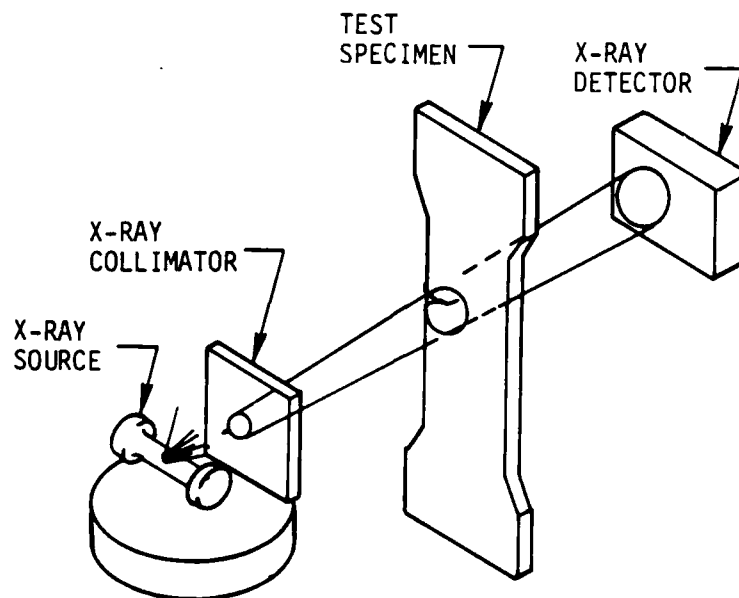


Figure 2-3. X-Ray Sensor System

References

1. Bachman, V. and D. Nuns, "Fatigue Crack Closure Evaluation with the Potential Method," Eng. Fract. Mech 11, 1979, pp. 61-71.
2. Rief, F. "Fundamental of Statistical and Thermal Physics," McGraw-Hill, NY, 1965.
3. Filter data sheets, Ealing Corp. Natick, MA, alternates:
Microcoatings, Westford, MA or Barr Associates, Westford, MA.

3. PROGRAM PLAN

The primary objectives of the Phase I program were to experimentally evaluate both the laser and x-ray approaches discussed in the previous section and to select the most viable approach to incorporate into an automated fatigue crack measurement system.

The program plan that was followed is shown in Figure 3-1. This plan is a deviation to the originally proposed plan to only experimentally verify the selected approach. The revised plan in Figure 3-1 included experimental verification of both the laser and x-ray approach and we believe this has led to a more realistic selection.

A programatic report on each task of the revised program plan follows; the technical results of these tasks appear in Sections 4, 5 and 6 of this report.

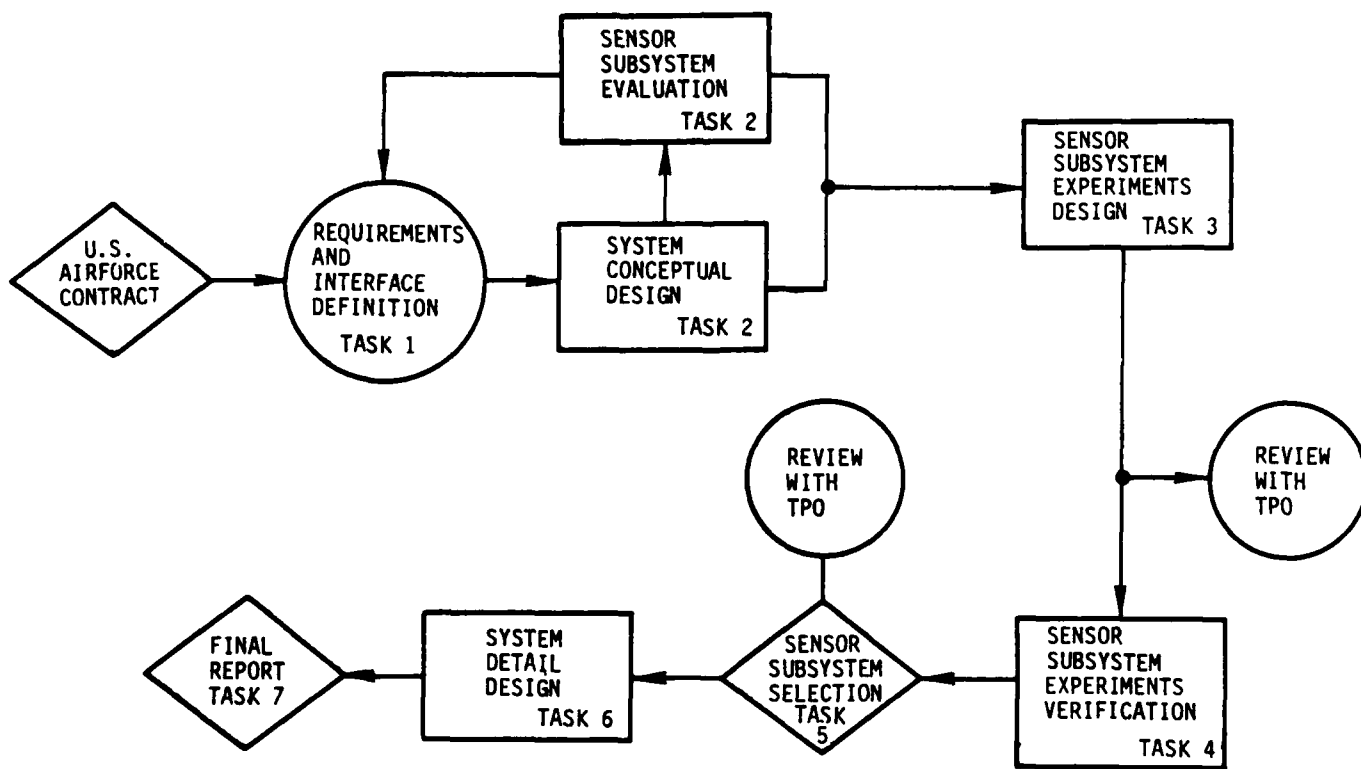


Figure 3-1. Program Plan

Task 1: Requirements and Interface Definition

The Principal Investigator, the Air Force Project Engineer and the head of the Fatigue Testing Laboratory met on 3 September 1987 and we reviewed a previously submitted list of detailed interface and requirements questions. We were provided with a contact at Research Inc. (RI) the selected oven contractor. RI was contacted and provided Foster-Miller with a set of oven interface drawings. The technical requirements and interfaces are discussed in Section 6.1.

Task 2: System Conceptual Design and Sensor Subsystem Evaluation

The proposed line scan conceptual design was reviewed and an imaging approach was reconsidered. Advances in available digital image processing technology had improved significantly since our proposal was written so we did not want to preclude this approach. Both laser and x-ray sensors remained our leading candidates so our conceptual design was revised to include the possibility of imaging in these two modalities. The revised conceptual design was then evaluated under the performance and interface requirements established in Task 1 to assure compatibility. The laser and x-ray approaches are discussed in Section 2.

Task 3: Sensor Subsystem Experiments Design

Laser and x-ray experiments were independently designed to demonstrate the feasibility of the conceptual design approach of Task 2 and that the sensor approaches were capable of meeting the performance and interface requirements of Task 1.

Once confidence in the experimental approaches was established detailed laser and x-ray experiment procedures were written, reviewed and sent to our technical monitor on 2 October 1987 for review.

Task 4: Sensor Subsystem Experiments Verification

The laser and x-ray experiments defined in Task 4 were conducted in the laser laboratory at Tufts University and at the Arnold Greene Testing Laboratory, respectively, in accordance with the detail test procedures generated in the previous task.

The laser and x-ray images that were generated were digitized on a laboratory scanning image digitizer at Hologics, Inc. The experiment results are presented and discussed in Section 4.

Task 5: Sensor Subsystem Selection

The digital images generated in the previous task were evaluated by computer to determine the precision of an automatic crack length measurement that could be achieved. On the basis of these data and an assessment of the difficulties experienced in each experiment the laser approach was selected as the sensor system to be implemented in a Phase II program. The experimental results, our selection and basis for selection was presented to WPAFB on 13 January 1988. This selection is presented and discussed in Section 5.

Task 6: System Detail Design

A detail system design was done based on the laser approach selected in the previous task and using the digital image processing considered in our conceptual design task. This detail system design is presented and discussed in Section 6.

Task 7: Final Report

A report discussing all the work done in the previous tasks has been prepared and is presented in this document.

4. EXPERIMENTS AND RESULTS

The experiments conducted on this project had a two-fold purpose:

- Demonstrate that both laser and x-ray approaches are feasible
- Determine if either approach has an advantage over the other in light of actual experience.

For the most part, these two experiments were carried on independently by separate project personnel who tended to champion their approach. In both cases, data were gathered photographically. This allowed a common method of comparison and digitization to quantify crack resolution.

4.1 Laser Experiments

The goal of this laboratory work was to show that a baseline crack in a specimen at 2,000°F can be imaged with the aid of laser light and a narrow band-pass filter. This was approached in two stages. The first was a series of room-temperature tests using a small He-Ne laser and a film camera. These tests were conducted to determine optimum illumination and viewing angles to obtain highest crack contrast. Work at room temperature permitted the examination of many variables without the difficulties of working with a heated sample in an off-premises laser laboratory. The second stage was the testing of an actual heated specimen using the argon-ion laser and narrow band-pass filter. With the experience gained from the room-temperature tests the tests at 2,000°F were carried out quickly and efficiently.

4.1.1 Room-Temperature Tests

We designed a room-temperature experiment to show that a hairline crack in a metal sample can be imaged with a laser, and to explore photographic and illumination variables. The test specimen, provided by the Air Force, was a partially cracked Inconel 718 sample 0.38 in. thick as shown in Figure 4-1. The specimen was prepared by loading to the same tension experienced when

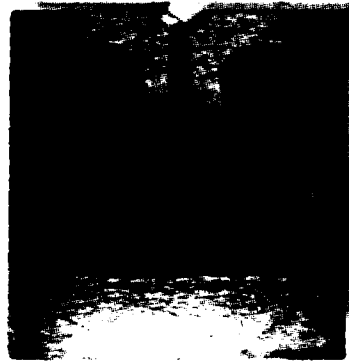


Figure 4-1. Inconel Specimen

it cracked and inserting a wedge to hold the crack at that opening. This would closely simulate the fatigue testing environment when the crack would be observed in real-time under load.

Figures 4-2(a) and 4-2(b) depict two variations of our setup. Figure 4-2(a) shows the object plane (the sample) to be parallel to the image plane (35 mm film), while Figure 4-2(b) shows the object plane to be tilted at an angle δ from the plane parallel to the image plane. Though different in orientation, both setups contain a cracked test specimen, a camera arrangement, a small 0.95 mW HeNe laser, and a beam expander. The beam expander lens was employed such that the beam covered the entire crack. (The diameter of an unexpanded HeNe beam is roughly 1 mm.) The camera arrangement contained the following:

- Olympus OM-1 body (35 μ m)
- Olympus Auto Bellows
- Olympus Auto-Macro 135 mm F4.5 lens
- Skylight (1A) 55 mm filter
- Metal mount plate.

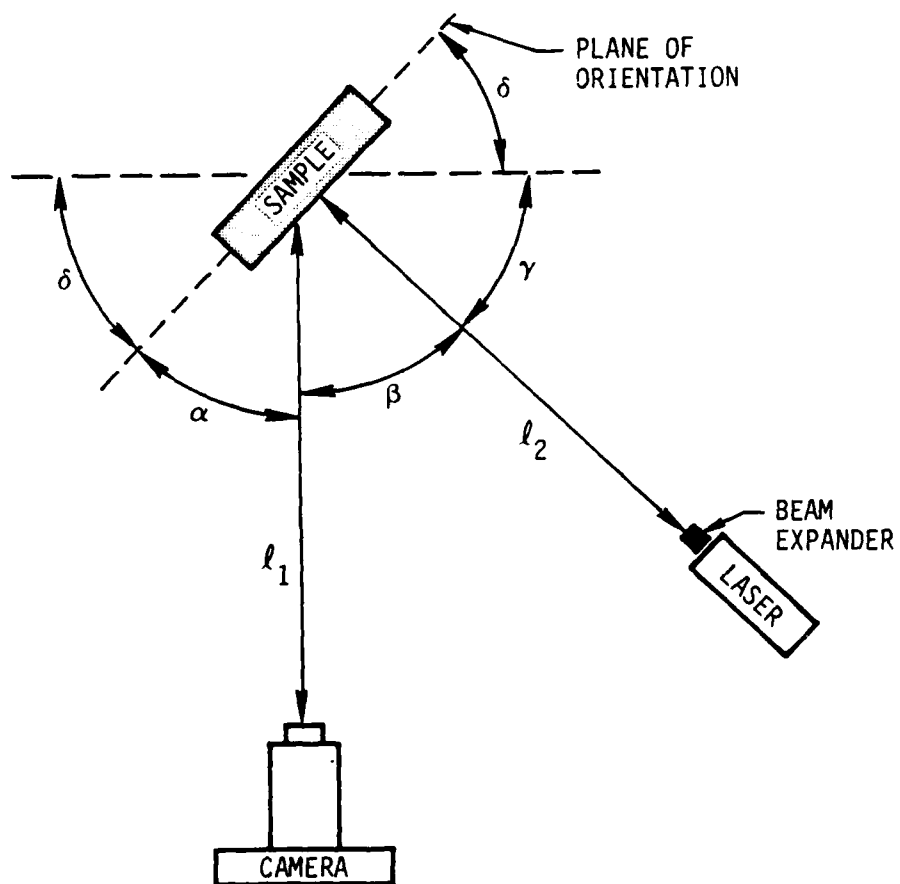
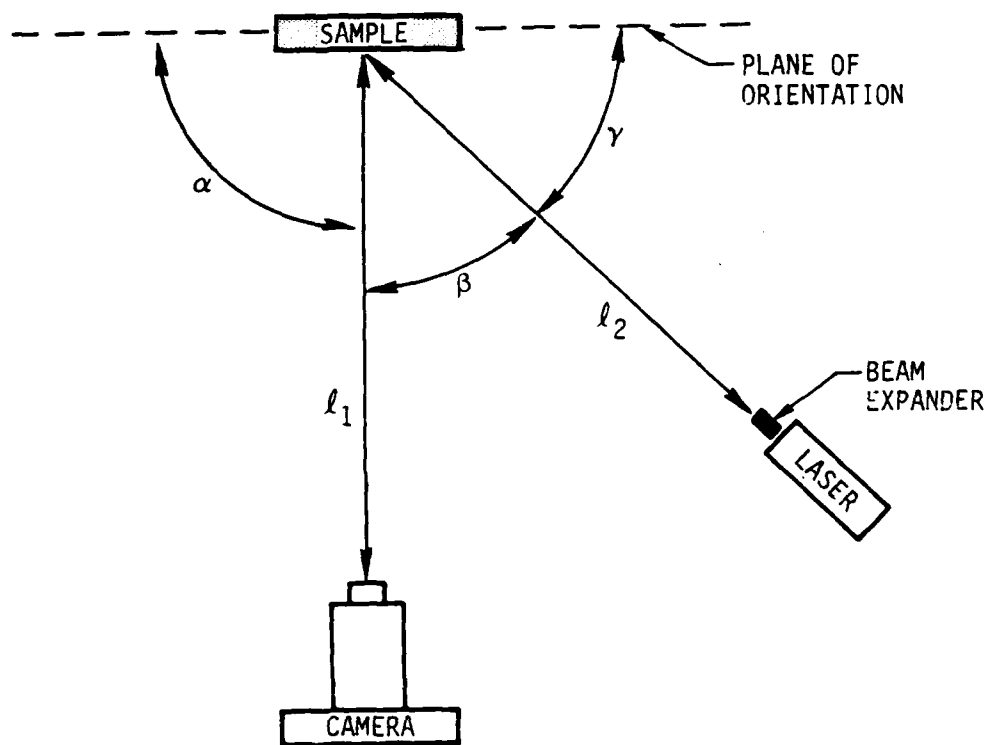


Figure 4-2. Laser Room Temperature Test Configuration

We used a heavy aluminum plate as a base for our camera arrangement to provide stability when taking long exposure pictures. The skylight filter was used strictly to protect the camera lens. The Olympus OM-1 body is a standard SLR 35 mm camera which contains a lightmeter that can be viewed when looking through the viewfinder. The Olympus Auto Bellows and the Olympus Auto-Macro 135 mm F4.5 lens provide high quality macro photos at magnifications of 1:1 while also offering a comfortable working distance.

For instant processing during experimental work, we used Polaroid PolaPan 35 mm instant black and white slide film (ASA 125). By developing the film with the Polaroid 35 mm Auto Processor we were able to see our results immediately. Kodak TMax Professional Film (ASA 400) was used for photography not requiring quick turnaround.

Procedures were simple and straightforward. Essentially, it involved bracketing the exposures of the sample illuminated by the HeNe laser for different orientations of the sample. This was done in a darkened room.

Changing the orientation of the sample simply refers to varying:

- Tilt angle δ (see Figure 4-2)
- The tilt of the sample relative to its plane of orientation
- The side that the sample rests on (i.e., whether the crack is perpendicular or parallel to the plane of orientation).

Bracketed exposures were required because of the difficulty of using the internal light meter with localized laser illumination. Thus, by picking an F number and choosing several different aperture speeds for that F number, we were able to ensure proper lighting for a few frames. Recalling that we were using ASA 125 film, we knew that the aperture speeds would range from 1 sec to 1/60 sec relative to the aperture size. Typical exposures (F/# and shutter speed) which gave best image with 0.95 mW HeNe illumination were: 4.5 and 1/8 sec, 11 and 1/4 sec, and 16 and 1/2 sec.

The other variable was magnification (the ratio of the object size to the image size on the film). Ideally, we wanted a magnification of 1:1 so as to permit precise measurement of the crack. Later on, we will see that this was not always practical. Varying the magnification simply meant varying the distance from the object to the lens (object distance), as well as the distance from the image to the lens (image distance). We were able to determine the proper object and image distance from tables provided by the Olympus Auto Bellows Operating Instruction booklet.

After these preliminaries we showed that high contrast illumination of a hairline crack could be produced with just a 0.95 mW HeNe laser. The best results were obtained when $\delta = 0$ (i.e., $\alpha = 90$ deg) and there was minimal tilt in the sample relative to its plane of orientation. (The sample used was labeled FF3 and provided by the government.) By having the object plane parallel to the image plane, we were able to achieve the best focusing. As δ increases and the relative tilt in the sample increases, the length of crack within the depth of focus decreases.

The only variable left in this experiment was the positioning of the laser relative to the plane of orientation of the sample as well as to the camera position. As the laser grazes the surface of the sample, the light is reflected by any small imperfections (i.e., hairline crack) in the sample. With grazing illumination the viewer perceives the crack as a bright streak on a dark background (see Figure 4-3a). With normal illumination, the viewer perceives the crack as a dark line on a bright background (see Figure 4-3b). We found the second method for viewing the sample to be the best method for the following reasons:

- By choosing the second method of laser alignment, there was a greater margin in positioning the laser. Positioning the laser beam very nearly parallel to the plane of the sample required a great deal of adjustment



a) BEAM PERPENDICULAR TO SAMPLE



b) GRAZING BEAM

Figure 4-3. Specimen Illuminated with HeNe Laser Beam

- With the laser beam normal to the sample, a bright background was achieved, which gave the crack depth as well as location. Using grazing incidence provided a bright crack against a dark background which yielded sharp contrast, but poor depth.

We concluded that normal incidence was the preferred method.

4.1.2 Hot Tests

The Air Force advised against heating the Inconel specimen to 2,000°F. A substitute specimen was machined in a local shop from 304 stainless steel. This was partially cracked by the Air Force in the WPAFB fatigue testing machines and returned to us. Figure 4-4 shows this specimen after testing. A wedge was used to open the crack or with the previous Inconel specimen. Also note that location of the thermocouple probe which was used to measure specimen temperature.

The method chosen to heat the sample was straightforward. We built a very small compact furnace out of firebrick for insulation. This furnace was designed such that a plumber's torch (heat source) could be inserted through a hole in the front and a thermocouple probe embedded in the side of the sample. By minimizing the size of the furnace, we achieved maximum retention of temperature. As soon as a picture was to be taken, the torch was shut off, the front door opened, and the picture taken. One had roughly 10 sec before the temperature of the sample fell by about 100°F thus adjustments of the camera were made prior to the taking of the pictures. Initially we positioned the camera such that the magnification was 1:1. This meant that the camera lens was roughly 9.1 in. from a 2,000°F source. We deemed this to be too close for the camera's safety. Thus, the camera was pushed back to about 14.4 in. yielding a magnification of 1:2, which proved adequate for the precise metrology method.

With these preparations, we were ready to try imaging the crack when heated to 2,000°F and illuminated by an argon ion laser, while having the thermal radiation filtered out by a narrow band filter as discussed earlier. The argon ion laser and laboratory space were provided by Tufts

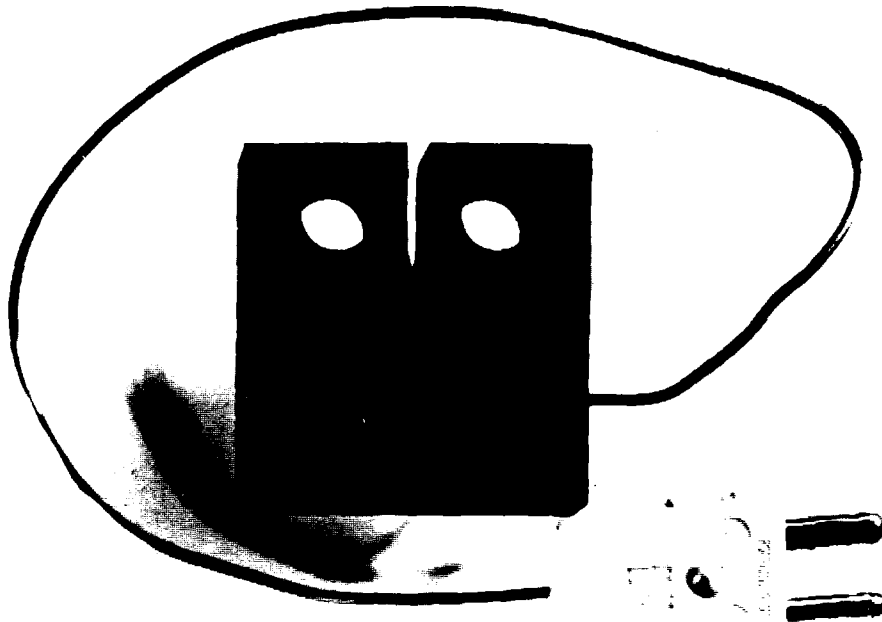


Figure 4-4. Stainless Steel Specimen with Thermocouple Probe

University. This investigation was broken down into five steps, each recorded photographically:

- (1) Sample at room temperature with laser
- (2) Sample heated to $2,000^{\circ}\text{F}$ with no laser and no filter
- (3) Sample heated to $2,000^{\circ}\text{F}$ with laser and no filter

(4) Sample heated to 2,000°F with laser illumination and narrow band filter installed

(5) Different angles of laser illumination.

Step (1): The setup of this experiment was essentially the same as Figure 4-1, except that the sample was within a furnace and the laser being used was a coherent model Innova 90 6-watt argon-ion laser. The method of bracketing was unchanged from the previous experiment. The output beam power was initially 330 mW. Near the output of the laser, the beam was split, thus leaving the detectable output power at 165 mW. We estimated that at the sample's surface the beam power was $100 \text{ mW} \pm 25 \text{ mW}$. For this portion of the experiment we used the Inconel specimen provided by the Air Force.

All room-temperature experiments were done with the laserbeam normal to the sample, consistent with our previous results for best data. Specifically for our set $\beta = 26.57 \text{ deg}$. The magnification was 1:2 for the entire series of argon illuminated photographs. Though there was no heat present, we wanted to keep the experiment as consistent and uniform as possible.

Step 2: Next we heated the 304 stainless steel sample to 2,000°F and observed it without any argon-ion laser illumination or narrow band filtration. We photographed the glowing metal in its own radiation as in Figure 4-5. We were vaguely able to observe the crack with moderate contrast. The crack was glowing slightly brighter than the rest of the metal sample. This phenomenon is well known in the theory of black-body radiation. The piece of metal acted as an isothermal enclosure for the crack. Within the crack a radiation field existed which was at thermal equilibrium with the walls of the crack and therefore appeared brighter than the outer surface. Black-body radiation field is independent of the shape of its cavity. Furthermore, the radiance L from the crack is independent of position and observation direction. This also explains why this effect was not as noticeable at cooler temperatures. This phenomenon

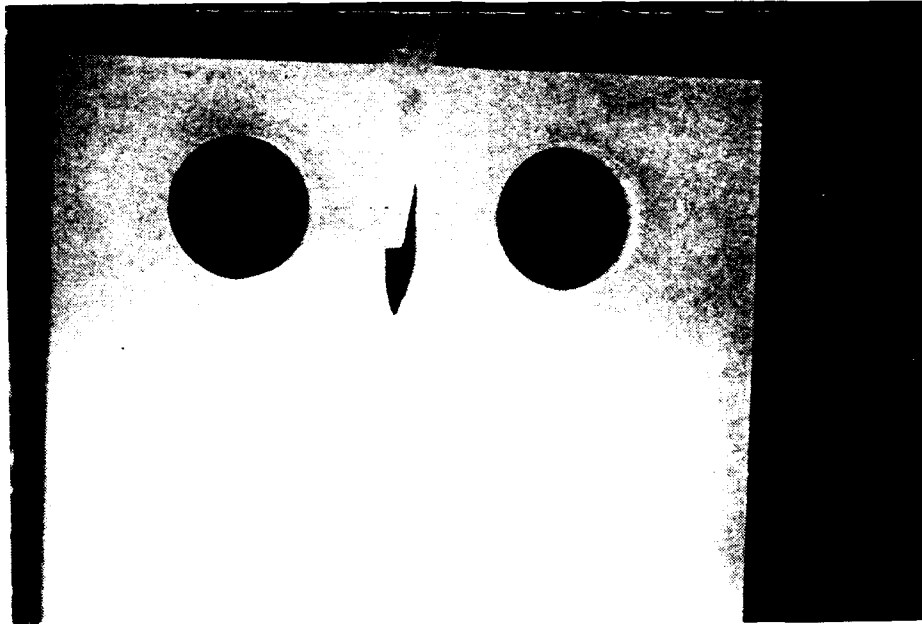


Figure 4-5. Self-Radiation only at 2,000°F

will be less apparent in an internally heated oven which will present a far more isothermal environment than our experiment.

Step 3: After completing the previous portion of the experiment, we proceeded to repeat it, but this time with argon-ion laser illumination added to the thermal self-radiation. The crack appeared as a faint dark line (see Figure 4-6). The contrast here was not very good, and the image was rather fuzzy. What we observed here was an example of Kirchoff's law. That is, a good emitter of radiation is also a good absorber of radiation. As shown before, the hairline crack in the sample was (relatively) a good emitter of radiation. With an argon-ion laser incident on the crack, it becomes a relatively good absorber.

Step 4: Next, we inserted the narrow band filter, Figure 4-7, over the camera lens. As expected, it blocked out most of the thermal radiation.

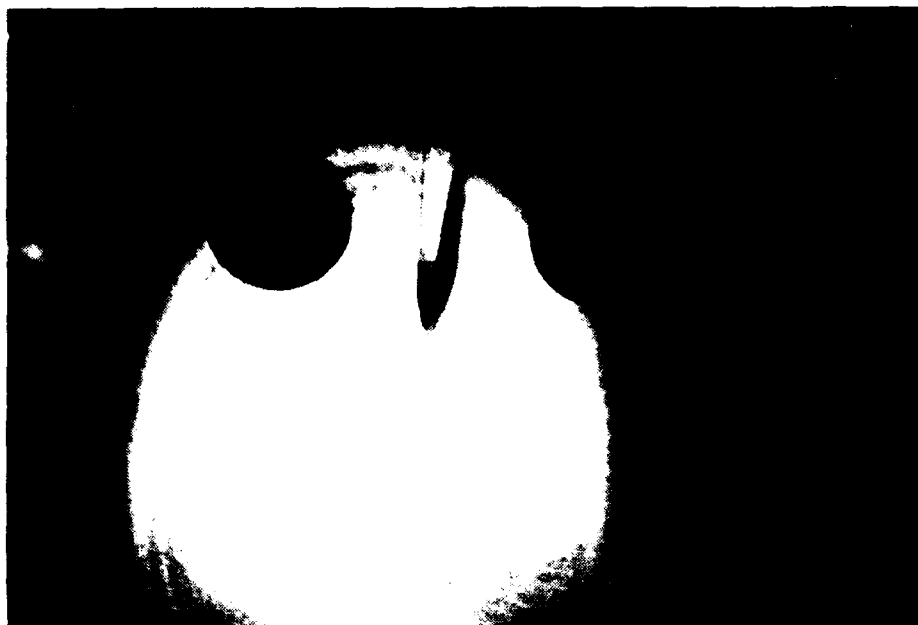


Figure 4-6. Specimen at 2,000^oF Illuminated by Argon-Ion Laser

The crack now appeared as a dark line, but the contrast was greatly enhanced (see Figure 4-8). Also, the image of the crack was much sharper. It is clearly easier to discern the entire crack from end to end.

Step 5: Though we had already determined that the best positioning for the laser was when $\gamma \gg \beta$, we again experimented with different positionings of the laser. First, the laser was positioned at $\beta = 65.7$ deg. Instead of discussing Steps 1, 2, 3 and 4 (as described before), we will only discuss part 4, since that is the one which concerns us. At $\beta = 65.7$ deg the crack appeared as a dark line, yet it was not as sharp as that found when $\gamma \gg \beta$. Since the light was incident at a grazing angle, all of the defects on the surface of the sample were enhanced. As a result, it was more difficult to decipher the boundaries of the crack as

ANDOVER CORPORATION

SPECTRAL ANALYSIS

TEST INSTRUMENT
SPEX 1.26 METER

TEST TECHNICIAN
D. ANDERU

DATE
07 OCT 12

CUSTOMER NAME
FOSTER-MILLER INC

JOB NUMBER
FM-9524

PART NUMBER
400FS03-50

SERIAL NUMBER
01

CENTER WAVELENGTH
4884.00 Å

BANDWIDTH (FWHM)
29.5000 Å

FWHM COORDINATES
4869.25 Å
4898.75 Å

PEAK TRANSMISSION
54.9373 %

AMBIENT TEMP.
29 DEGREES C

ANGLE OF INCIDENCE
0 DEGREES

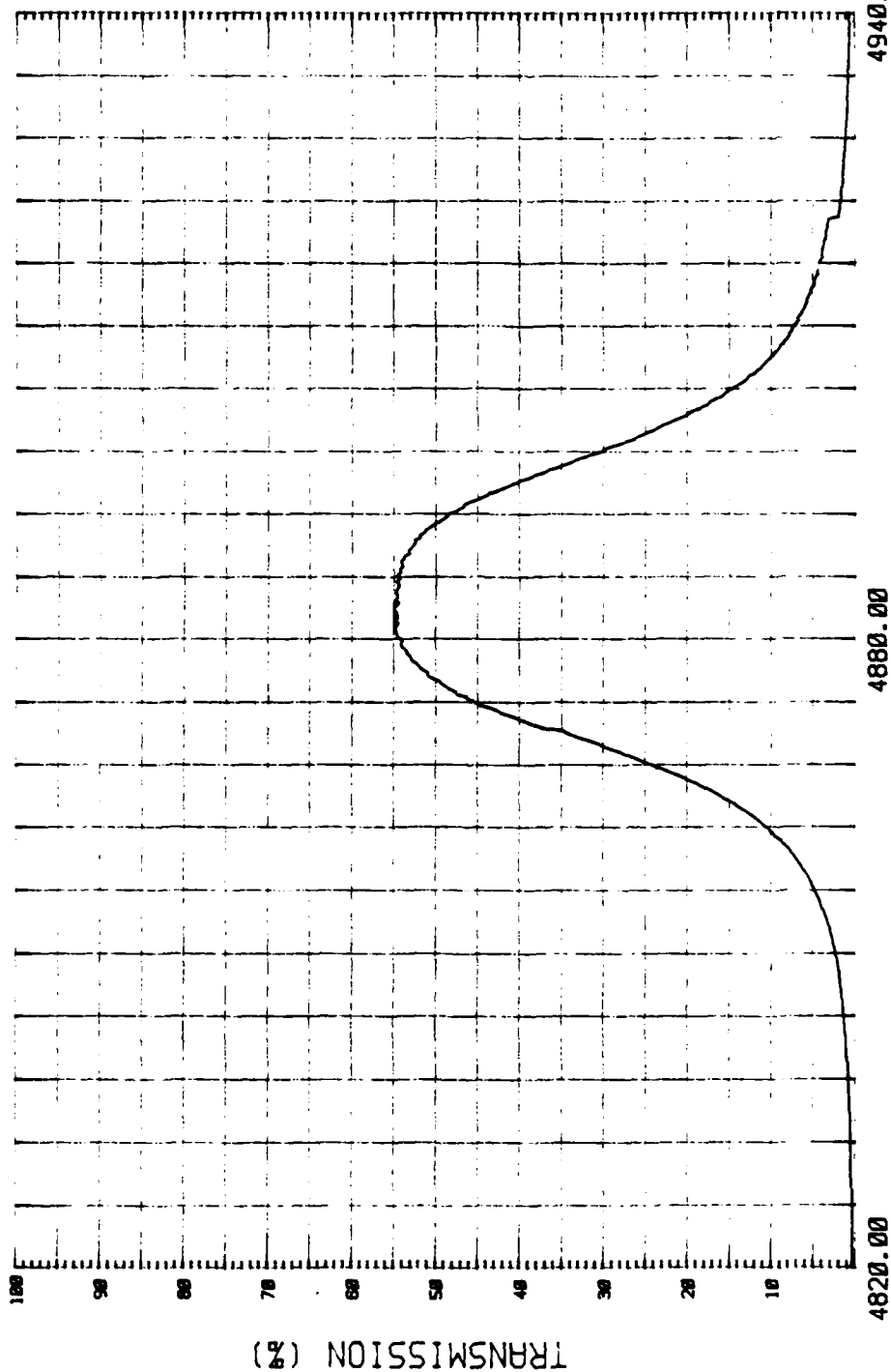


Figure 4-7. Narrow Band-Pass Filter Characteristics,
Centered on Argon-Ion Wavelength

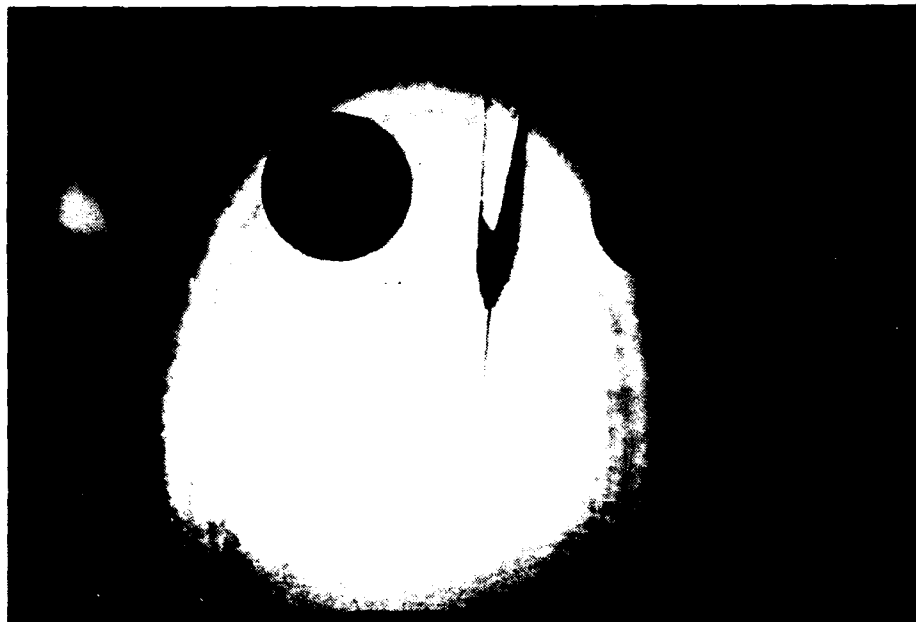


Figure 4-8. Specimen at 2,000°F Illuminated by Argon-Ion Laser
Viewed Through Narrow Band-Pass Filter

compared to when $\beta = 26.57$ deg. Clearly this method does not yield enough contrast for imaging a hairline crack.

Finally, we attempted directing the laser beam through the crack from behind without much success. This method requires very precise alignment. Moreover, the size of the crack must be larger than the wavelength of the laser beam. Also, the crack is not necessarily smooth and normal to the sample surface; hence, a clear path may not exist.

4.1.3 Results

As expected, the best crack contrast and sharpness is achieved for hot specimens when the specimen is illuminated by the laser and viewed through the filter. Both laser beam angle and view angle should be as near perpendicular to the sample as practical. The laser experiment results are summarized on Table 4-2. Quantitative data on crack length determinations is presented in Appendix A.

4.2 X-Ray Experiments

The main advantage of an x-ray measurement technique is in its complete immunity from any thermal noise measurements (which contribute to background in the visible wavelength detection band), and its inferred ability to measure a position over the entire front of the crack advance.

The primary concern with the x-ray approach is crack detectability in situations where the crack is not orthogonal to the detector plane.

To verify this approach, a set of feasibility experiments were designed with an x-ray system. While the implementation of an automated system would be with a real-time x-ray detector, for test of feasibility digitized x-ray film images of the crack under different orientations provides good calibration of the method.

4.2.1 X-Ray Testing

The x-ray testing was performed at Arnold Greene Testing Laboratories, Natick, MA. Foster-Miller program personnel on-site directed the test assisted by testing laboratory technicians. The x-ray source was a GE Model OX250 with a 3 mm focal spot. Prior calculation showed that excellent geometric sharpness could be achieved with a 4 mm x-ray source placed 27.5 in. from photographic film in contact with the rear side of the specimen. With smaller focal spots the distance can be proportionally shorter while maintaining image sharpness. Previous calculations indicated that an x-ray source voltage of 125 kV was a good candidate for penetrating the 0.38 thick Inconel specimen.

As it turned out, energies between 100 kV and 125 kV were most appropriate for making film exposures of the crack. A series of such exposures along the line of (Figure 4-9) (test setup) were made. A listing of the actual exposures and conditions is shown in Table 4-1. A photograph of the experimental holding block setup is shown in 4-10. the block is designed so that it could be tilted to a preset angle with respect

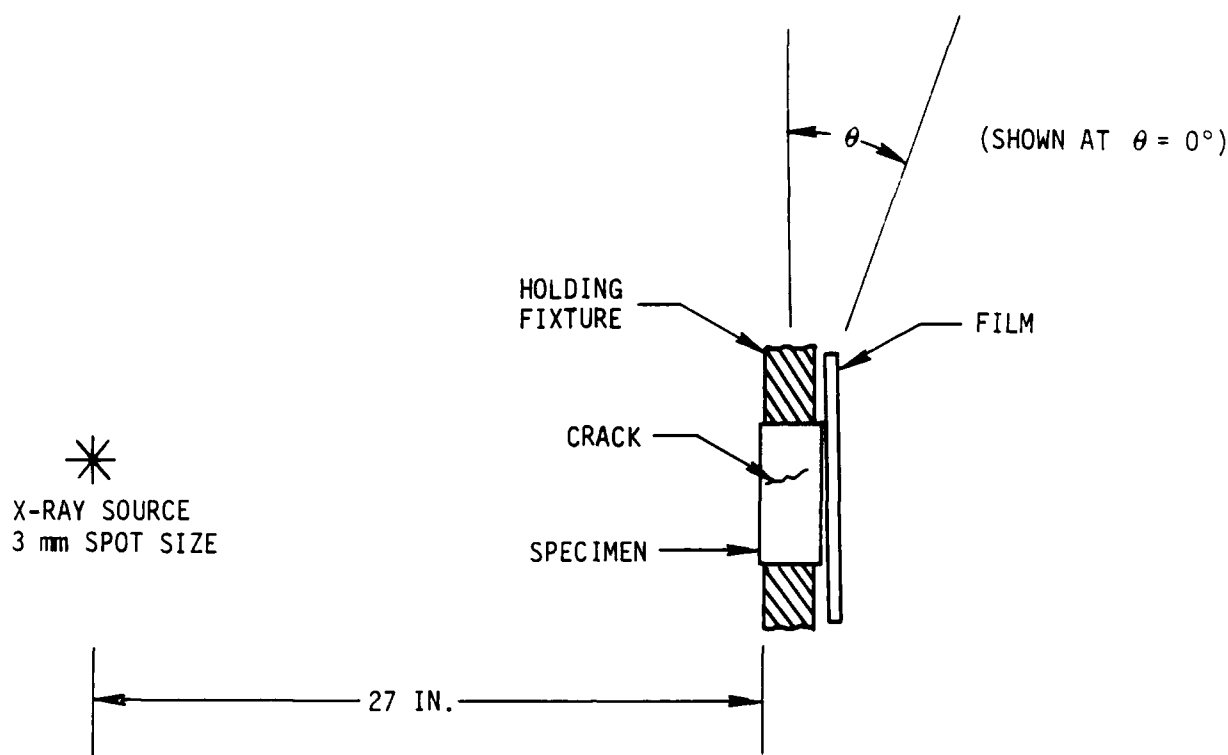


Figure 4-9. X-Ray Test Setup

to the x-ray beam. Thus, film exposures at the various angles could be made.

Exposure times and energies were initially made according to prior calculations. The aim was to produce a mid-range of film density of about 2.5, a value well-suited to digitization by conventional means. Empirical corrections to the calculated exposure times and energies were then made, resulting in the exposures shown in Table 4-1. The geometric unsharpness inherent in the test setup (a function of focal spot size, geometric configuration, and detector) was better than the desired 0.001 in.

4.2.2 Results

Visual examination of the radiographs clearly showed crack front definition (Figure 4-11) as long as the angle between the x-ray beam and the crack orientation did not differ by more than 10 to 15 deg. At higher

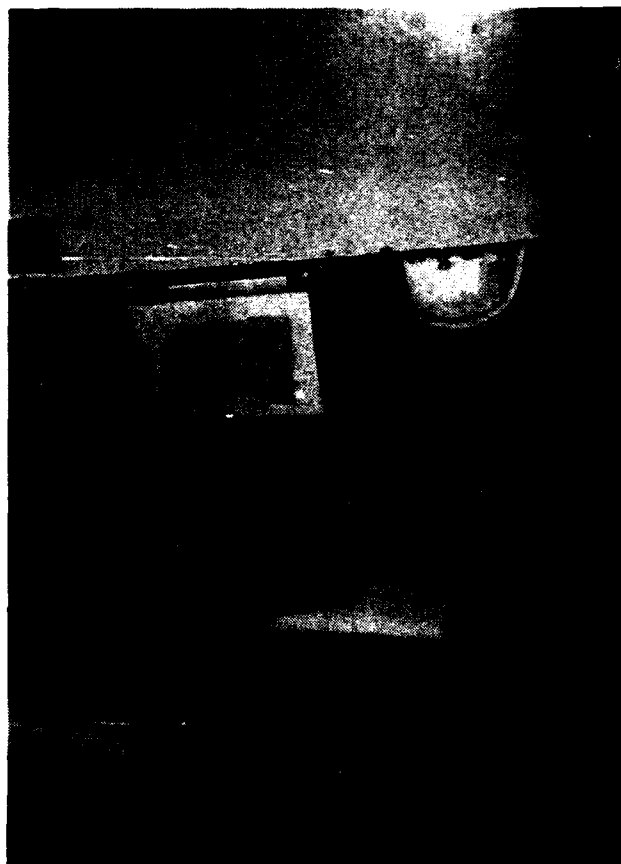
Table 4-1. Film Exposure Conditions

Film ID No.	Voltage kV	Current MA	Exp. Time (S)	Distance/ Distance/ (deg)	Film Type	Development
1 NL	125	10	90	27.0/0	Kodak M	11 min Kodak Mod. B
1	125	10	60	27.0/0	M	"
1A	125	10	48	27.0/0	M	"
2	125	10	48	27.0/50	M	"
3	125	10	48	27.0/10	M	"
4	125	10	48	27.0/20	M	"
5	125	10	48	27.0/30	M	"
5A	125	10	144	27.0/30	M	"
4A	125	10	144	27.0/20	M	"
3A	125	10	144	27.0/10	M	"
6	125	10	144	27.0/15	M	"
7	125	10	144	27.0/45	M	"
7A	125	10	450	27.0/45	M	"
7B	125	10	48	27.0/45	M	"
7C	125	10	15	27/45	M	"

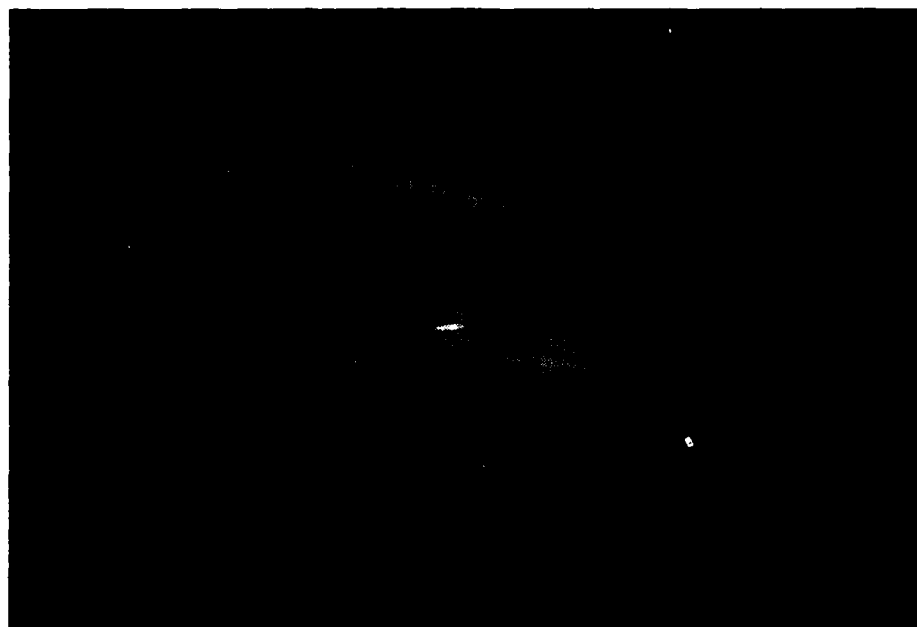
angles the location of the crack front was less pronounced. However, in practice crack angles would be expected to be oriented within less than 10 to 15 deg of the x-ray beam. The x-ray experiment results are summarized in Table 4-3. Quantative data on crack length determination are presented in Appendix B.

4.3 Reduced Data

Both the laser and x-ray tests produced data in photographic form showing the fatigue crack tip. The crack tip location was determined by

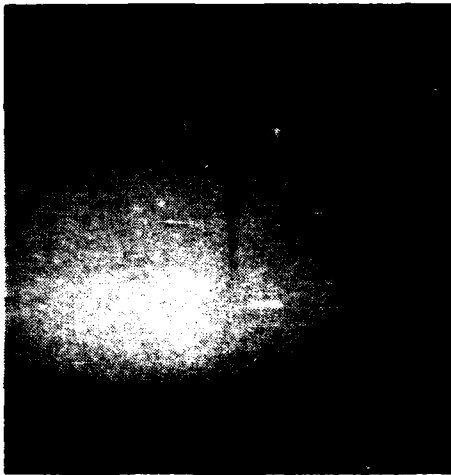


a) GEOMETRY WITH SPECIMEN TILTED

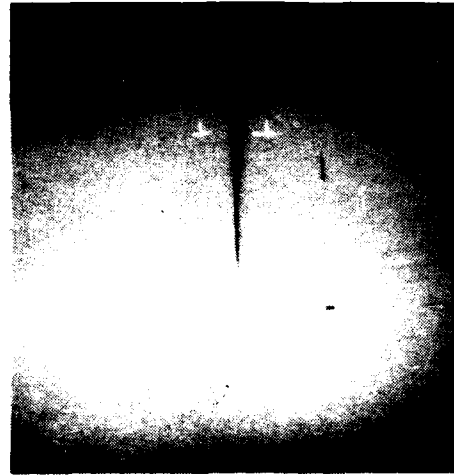


b) SPECIMEN HOLDER

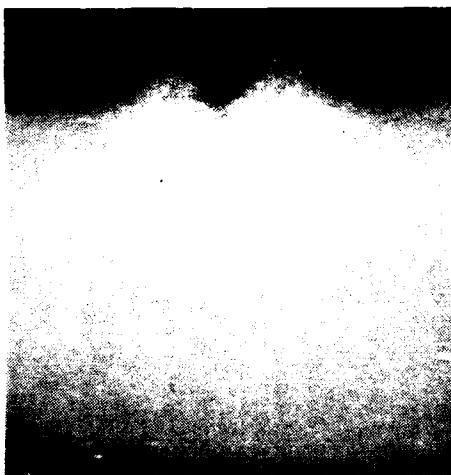
Figure 4-10. X-Ray Testing



0° ANGLE OF INCIDENCE



5° ANGLE OF INCIDENCE



10° ANGLE OF INCIDENCE



20° ANGLE OF INCIDENCE

Figure 4-11. Radiograph of Inconel Test Specimen

direct measurement and through image-digitization techniques. This latter method was employed because it is an essential component of the automatic measurement systems we had under consideration and therefore should be demonstrated during the Phase I program.

The image digitization was accomplished on a laboratory video scanning system at Hologics, Inc. in Waltham, Ma. The Hologic's scanner utilized a vidicon camera with automatic gain adjustment, resulting in the best visual presentation for each particular film image. The camera provided a standard video output of approximately 500 lines square. This was focused on an area of about 1 in. square, and thus, the effective spatial resolution was ± 0.001 in. The digitized array outputs were stored on 5-1/4 in. diameter diskettes, appropriate for off-line image processing and analysis at Foster-Miller.

The digitized laser and x-ray images are provided in Appendix A and B, respectively. The crack measurement results are presented in Tables 4-2 and 4-3 appearing in this section. Measurements were made by simply counting the number of pixels from the crack tip to the specimen edge and comparing this measurement to the diameter of the calibrated hole.

Table 4-2. Laser Experiment Data

Film Number	2,000°F Temperature	Laser Illum.	Filter	Measure (in.)*	Error (%)
2	X			1.288	42.0
3	X			0.916	1.2
4	X	X	X	0.927	2.4
5	X	X	X	0.915	1.1
*Actual measurement 0.905 in. from end of crack to edge of specimen Specimen 304 SS provided by Foster-Miller					

Table 4-3. X-Ray Experiment Data

Film Number	Angle of Incidence*	X-Ray Dose (RADS)		Measure (in.)**	Error (%)
		Crack	Surround		
1A	0	700	500	(3)	(3)
2	5	1100	500	0.809	0.9
3	10	700	600	0.836	21.0
4	20	500	400	0.619	23.0
5	30	500	400	—***	—***
*Angle off perpendicular to specimen **Actual measurement 0.802 in. from end of crack to edge of specimen ***Lack of reference measurement voided data Specimen FF-3 provided by USAF					

5. EXPERIMENT CONCLUSIONS AND RECOMMENDATIONS

The data from both the laser and x-ray crack detection experiments clearly indicate that both approaches are viable. A more extensive evaluation of these data was necessary to select one approach over the other.

5.1 Laser Experiment

The experimental results for the laser approach were actually much better than expected. The signal to noise was so good with the argon laser illumination that very acceptable data were obtained without the narrow band filtration. This implies that a narrow band filter system will be capable of much higher temperature operation. Or conversely, we can meet system performance requirements with a much lower power laser, hence lower cost. For this same reason we can use a broad band filter, which is easier to manufacture, lower cost and less susceptible to aging effects.

5.2 X-Ray Experiment

As expected, the experimental data (film) for x-ray beam angles within ± 5 deg of orthogonality with the specimen (essentially close to parallel with the crack face) was excellent. For angles up to ± 20 deg the data is marginal and above that, not useable.

5.3 Sensor Selection and Recommendations

On the basis of the above data the laser approach is the clear choice as it is evident the performance margins are much greater than with the x-ray approach. Implementation of a visible light system is also simpler, safer and less costly as the x-ray system would require additional shielding and interlocks to make it operator safe.

The x-ray system becomes more viable at the $4,000^{\circ}\text{F}$ and $5,000^{\circ}\text{F}$ temperatures discussed during the presentation of the experimental results. A

quantitative comparison of performance at these high temperatures is beyond the scope of this program.

The x-ray system also becomes more attractive if knowledge of the true crack front is desired rather than its position at the surface. However, one must compare such a system to a two-sensor laser system that views the specimen from both sides.

All things considered, we have presented the laser approach to the Air Force as our choice in the implementation of an Automated Fatigue Crack Measurement System. It is the design we present and discuss in the following section of this report and it is the design we will propose for a Phase II program.

6. SYSTEM DESIGN

Initially our system concept was based on manually locating a fatigue crack tip then automatically having the system follow and report the crack growth. Figures 6-1 and 6-2 show this concept as we proposed it. As a system, it is compatible with the use of either x-ray or laser beam sensors. We also expected that there would be cost advantages over a vision measuring system where appropriate software operates on a digitized video image to detect and monitor crack growth.

Two developments altered this perception since the submission of our proposal. First, a common system requirement will be to monitor two crack tips simultaneously on a single test specimen due to crack initiation methods. Second, the price of powerful machine vision systems has dramatically declined in recent years.

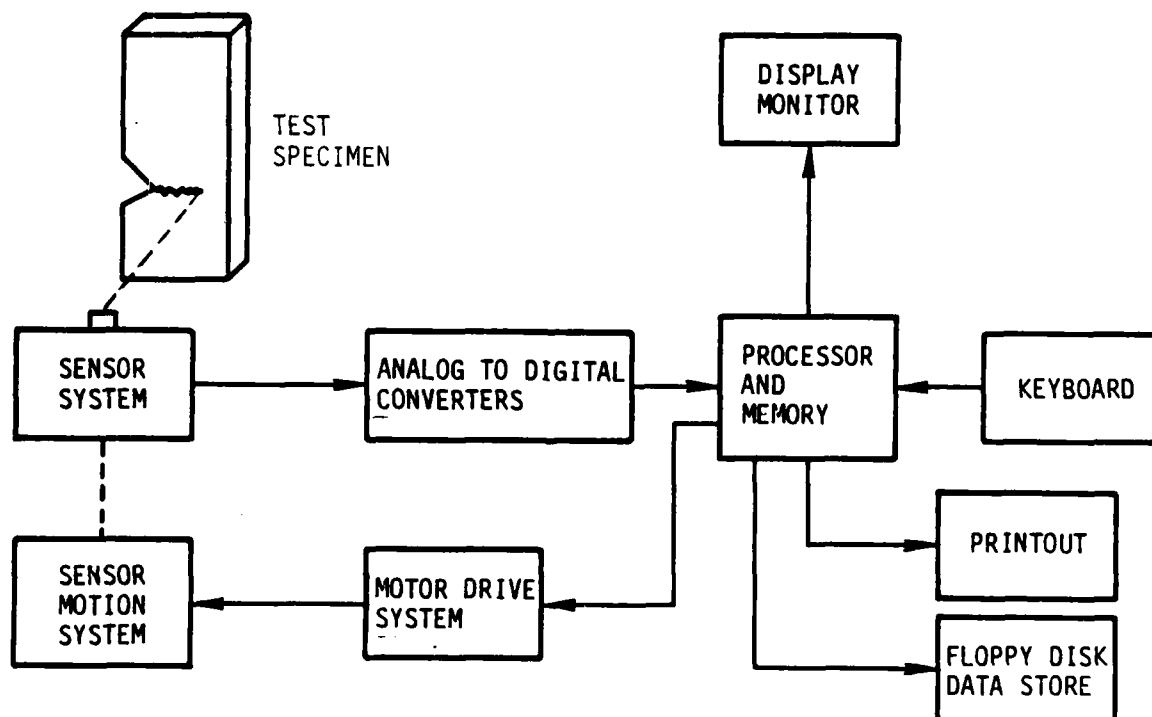


Figure 6-1. Proposed System Concept

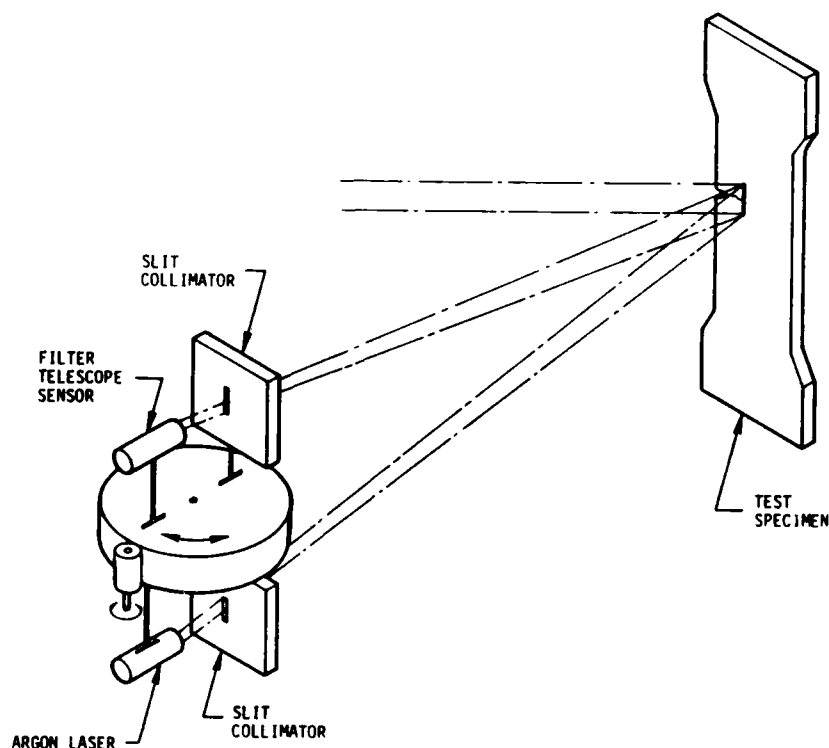


Figure 6-2. Proposed Line Scan Laser System

As with the original proposed approach, a machine vision system is compatible with either the laser/filter or x-ray method of crack detection. Both detector systems can produce a high-resolution visible image as was demonstrated in our experiments. These images are directly useable by a machine vision system which would then accomplish the crack detection and measurement through appropriate software and without the moving parts of the proposed line-scan system. Furthermore, the machine vision system will be simpler to use, eliminating the precise manual alignment of the line image (necessary to detect crack initiation). Future changes and expansion of operating modes will also be easier to implement on a software-based machine-vision system.

6.1 System Description

Figure 6-3 presents our revised design for an automated fatigue crack measurement system based on our selection of the laser/filter detection method and on a machine vision approach. This system design has been developed to

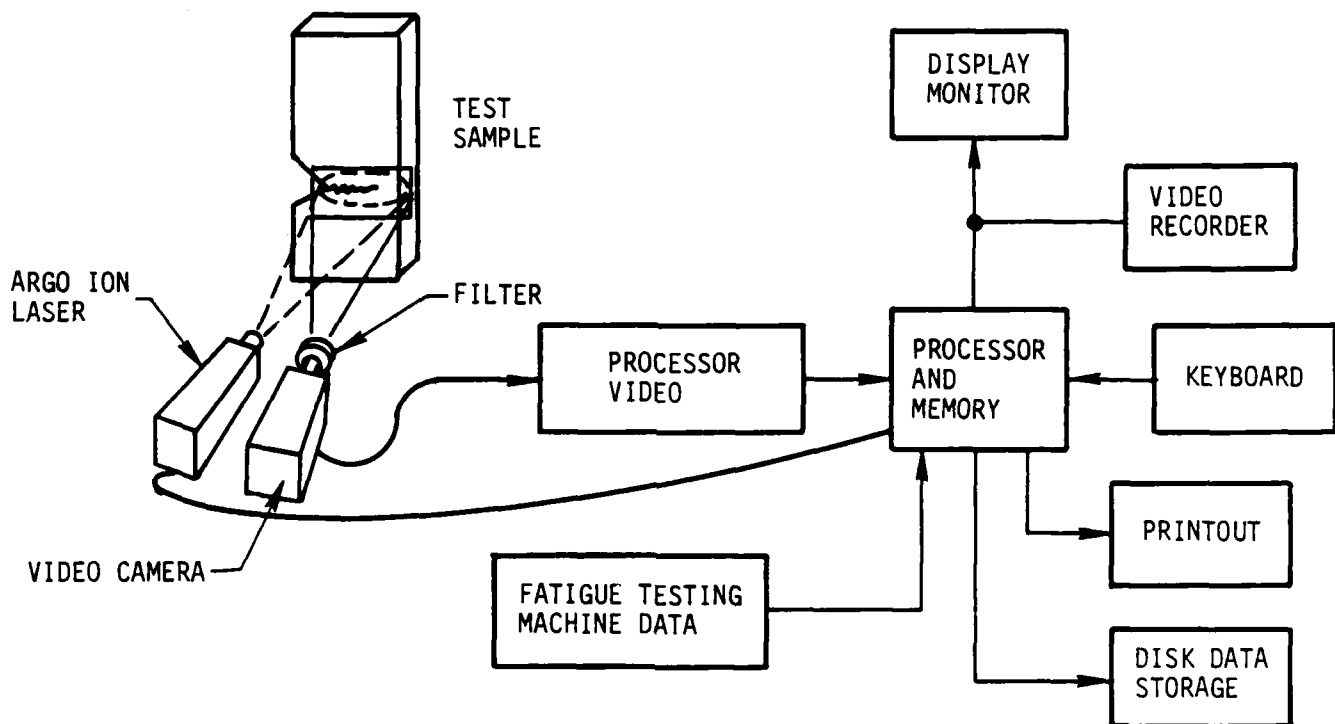


Figure 6-3. System Design Concept

the point of assessing accurate development and fabrication costs. Following subsections discuss key considerations and features of this design.

The system design is based on meeting the performance requirements as shown in Table 6-1 and on a number of interface factors determined in the course of the Phase I program. These factors include:

- Compatibility with the Specimen Oven currently being designed and fabricated by Research, Inc.
- Crack measurement in the vibration environment induced by the fatigue testing machine.

Table 6-1. Performance Requirements

SPECIMEN:	
• Material Min:	Aluminum, 0.050 in. thick
• Max:	Inconel 718, 0.5 in. thick
• Crack Resolution:	0.001 in.
• Crack tracking Speed:	0.030 in. per sec
• Temperature Range:	-50°F to 2,000°F
TEST MACHINE: (MTS, 2 Post, 100 Kp Frame Size)	
• Test Frequency:	0 to 50 Hz
• Oven Window:	4 in. x 1.8 in. quartz
ENVIRONMENT	
• Air Conditioned Laboratory	
• Clearance:	30 in. behind, 36 in. front

To assure compatibility with the specimen oven we obtained the following drawings from Research, Inc.:

- Material Test Radiant Heat Chamber D074380-001 dated 8-6-87
- Frontal View, Radiant Heat Chamber in Load Frame D074381-001 dated 8-6-87
- Top View, Radiant Heat Chamber in Load Frame D074382-001 dated 8-6-87

Our design, which is floor mounted, can perform with or without the oven and is compatible with the oven as defined by these drawings. Our only concerns are the operating temperature of the oven window, which is not defined, and possible specimen obstruction to a rear viewing camera due to the limited width of the oven's rear compliance gage port.

Both oven concerns are minor, but they will be addressed immediately at the start of the Phase II program when more detailed information on the oven will be available.

Real-time crack measurement in the vibration environment induced by the fatigue testing machine is helped considerably by the fact that the cracks typically propagate orthogonal to the testing axis of the machine. Discussions with the MTS Systems Corporation design engineers revealed that

machine motion in this direction is well below the 0.001 in. measurement resolution intended for our system. This motion remains a concern, however, and it is the prime reason we elected to isolate (floor mount) the crack measurement sensors from the fatigue testing machine and specimen oven. This system configuration is shown in Figure 6-4.

6.2 Vision System Description

The prime requirement of the vision system is a measurement resolution across the specimen of 0.001 in. A 4-in. wide specimen imaged by a good state-of-the-art 1000 pixel television camera, would yield a crack resolution of only 0.004 in. By introducing an optical system to form a folded image of

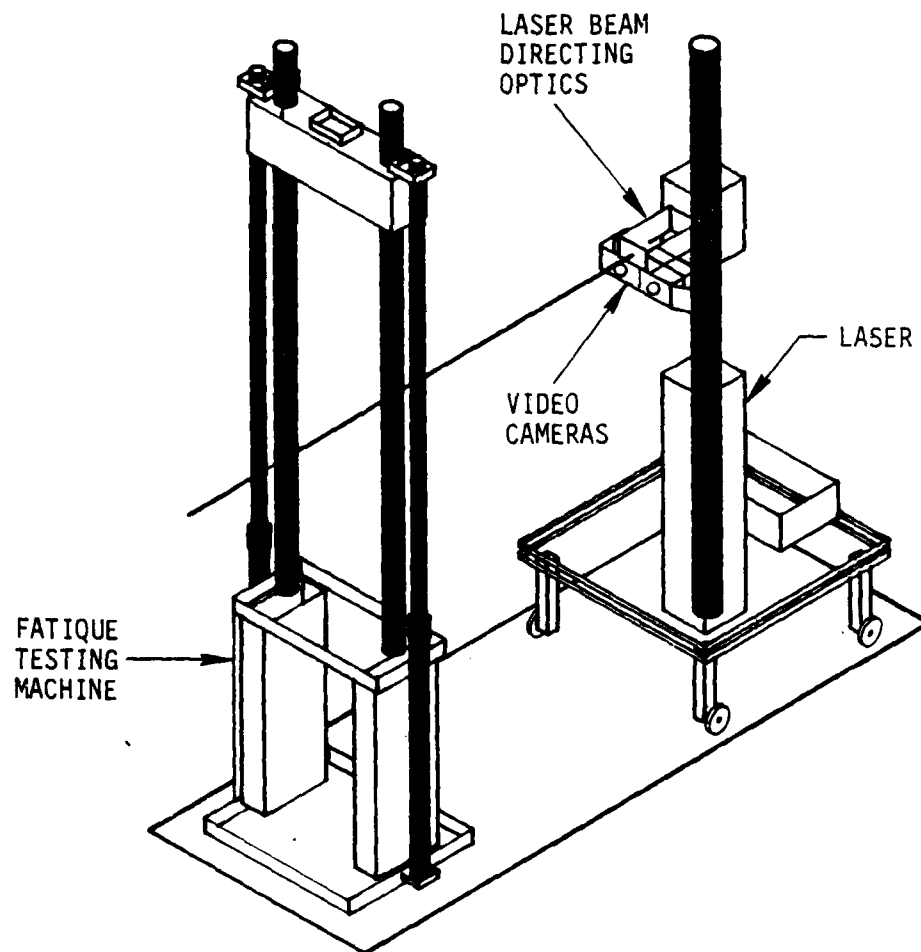


Figure 6-4. Crack Measurement System Mobile Sensor Subsystem Configuration

four segments of the sample (each segment would be 1 in. long with 1000 pixels and use about 1/4 of the height of the camera image). This could provide the required resolution using a single camera. However, a custom optical design is required.

Cost structure for vision systems is such that for a prototype system it is less costly to use four cameras imaging different segments of the test specimen than to design and build a custom mirror system. With this fact, we proceeded with a system design based on using a four camera vision system. In a production system the opposite would be true and we would proceed accordingly.

Foster-Miller has had corporate experience working with Foxboro/Octek, Inc. on applications of state-of-the-art vision systems. We have reviewed our performance requirements with Octek; an adaption of the Octek "Hawk Eye" system will meet these requirements as well as requirements for:

- Locating initiation of crack growth for more than one location
- Recording the progress of the crack tips
- Receiving correlative information from the testing machine on time, load, frequency and total cycles
- Processing this information and presenting the results in a format useful for Air Force testing laboratory personnel.

Figure 6-5 shows a typical Octek machine vision system packaged in NEMA enclosures.

6.3 Mobile Sensor System Description

The mobile sensor system carries the laser source and cameras, holding them in precise alignment, providing rapid postioning at any fatigue testing machine in the laboratory. Specifically it is shown in Figures 6-4 and 6-6 and contains:

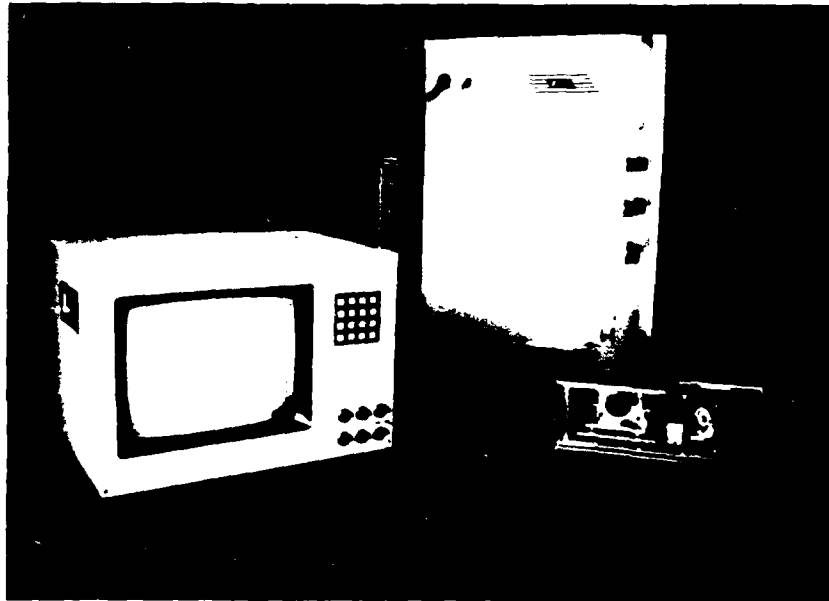
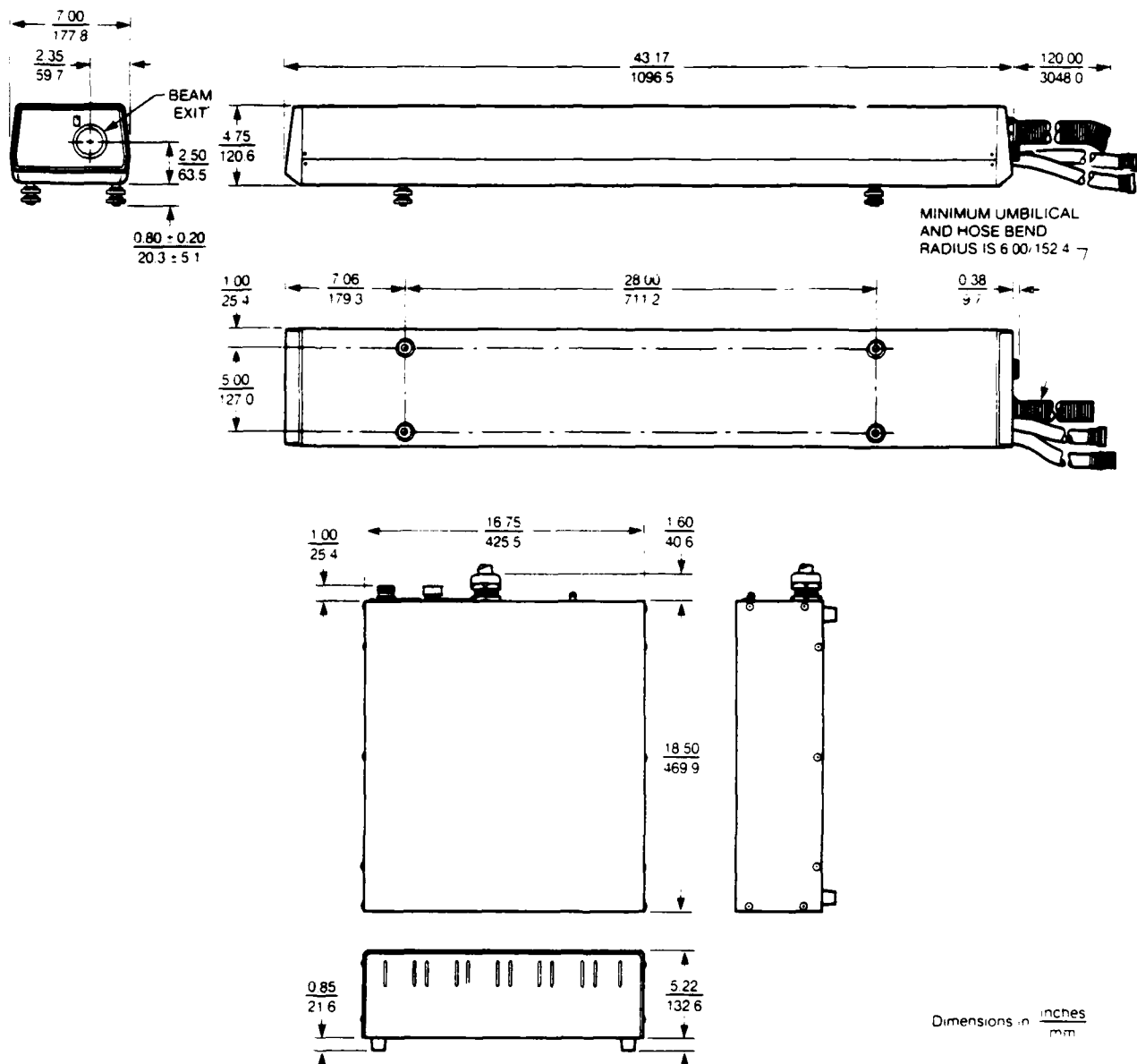


Figure 6-5. Typical Foxboro/Octek Machine Vision Equipment in NEMA Enclosures

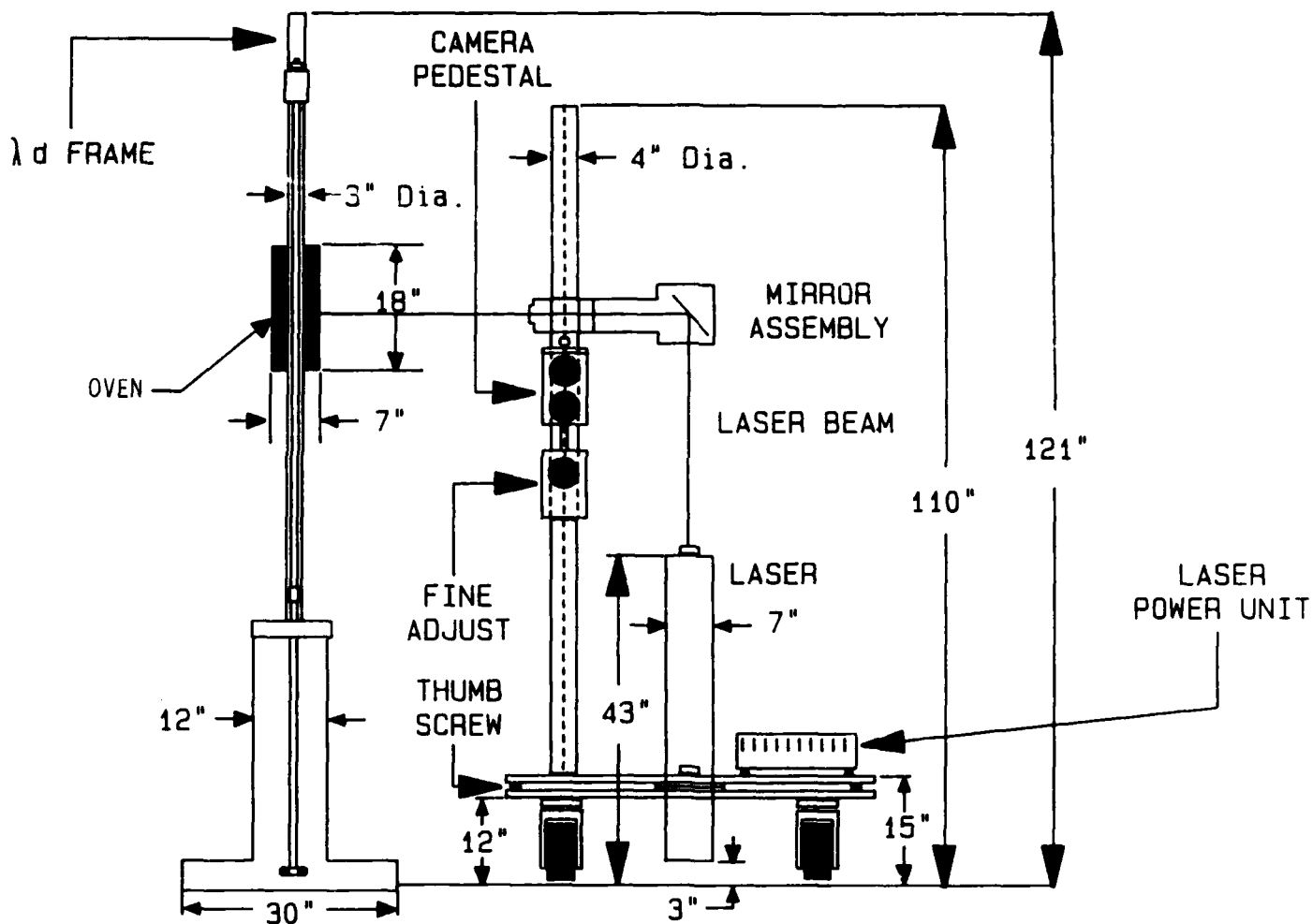
- The argon-ion laser, its power supply and its folding and focusing optics
- Four video cameras
- Rapid height and angular positioning pedestal
- Vibration isolation and leveling screws
- Mobile base with wheel locks.

As indicated in the previous section we decided to use four video cameras to achieve the 0.001 in. revolution and to mount them off the vibration testing machine for isolation. Further, the argon-ion laser is a sizeable, heavy (95 lb) piece of equipment (see Figure 6-6). For these reasons we selected a design approach that used a special cart that could be wheeled up to the front of a testing machinery providing rapid mobility and set up while maintaining the necessary precise alignment.



a) ARGON-ION LASER WITH POWER SUPPLY

Figure 6-6. Argon-Ion Laser



b) LAYOUT OF VIDEO/LASER CART WITH TESTING MACHINE

Figure 6-6. Argon-Ion Laser (Continued)

Special features of this cart are:

- Locking pneumatic tires hold the cart stationary and reduce any vibration levels from the floor which could affect accurate optical alignment
- A rigid 4-in. aluminum vertical support holds the adjustable video camera rack throughout the height range of interest for monitoring the test specimen
- An adjustable video camera rack holding the four cameras and allowing fine adjustments to align the specimen view position of each camera (this is done by watching the video monitor during adjustment)
- Vertically mounted laser requires only a single beam turning mirror to illuminate the specimen
- Weight of the laser and laser power supply helps keep the cart center of gravity low for stability.

The cameras and laser beam would be manually adjusted to view the test specimen through the quartz window on the oven, or viewed directly as in room temperature testing. This cart would be connected by an umbilical cable to a mobile, remoted control console holding the computer and display equipment. This approach allows considerable flexibility for various setups around the testing lab.

6.4 Simultaneous Crack Measurement From Both Sides

During the presentation of the experiment results, sensor selection and system design to WPAFB Laboratory personnel there was strong interest in simultaneous crack measurement from both sides of the test specimen.

The simplest implementation of two-sided measurement would be to duplicate the mobile sensor cart described in the previous section and provide for a

dual input to the image processing system. This would also be the most costly approach and may not be achievable within Phase II cost guidelines.

A trade study is being conducted into alternate means of achieving two-sided measurement that could be implemented within cost guidelines. Among the currently considered approaches are:

- A reduction in system resolution to ± 0.001 in. thereby requiring only 2 cameras per side
- A reduction in laser power and/or frequency, thereby reducing laser acquisition cost.
- Combining both side sensors on to one more complex cart but permitting the use of a single laser with a beam splitter and fiber optic transmission lines.

The results of this trade study will be reflected in our Phase II proposal.

6.5 Higher Temperature Measurement Capability

During the presentation to WPAFB laboratory personnel there was interest in extending the temperature range of the crack measuring system to $4,000^{\circ}\text{F}$, possibly even $5,000^{\circ}\text{F}$.

The excellent performance margins realized on the laser experiment at $2,000^{\circ}\text{F}$ would indicate that considerably higher temperature performance is possible. However the black-body radiation emitted by a specimen will increase exponentially with temperature and the peak radiation frequency will shift toward our current argon laser line.

As with the two-sided crack measurement, higher temperature performance is a tradeoff parameter with cost. The cost is not only associated with higher power/higher frequency laser performance but also with all the optical components that now must operate reliably in the vicinity of much higher temperature. These tradeoffs will be discussed in our Phase II proposal.

APPENDIX A

LASER EXPERIMENT DATA

The laser experiment data provided in Appendix A is summarized in the following table. The digital images that follow were generated directly from the photographic images presented in Section 4. Crack measurement was made by pixel counting from the crack tip to the edge of the specimen. Pixel calibration was accomplished by pixel counting the diameter of the specimen holes and comparing this count to the actual measurement of the hole diameter.

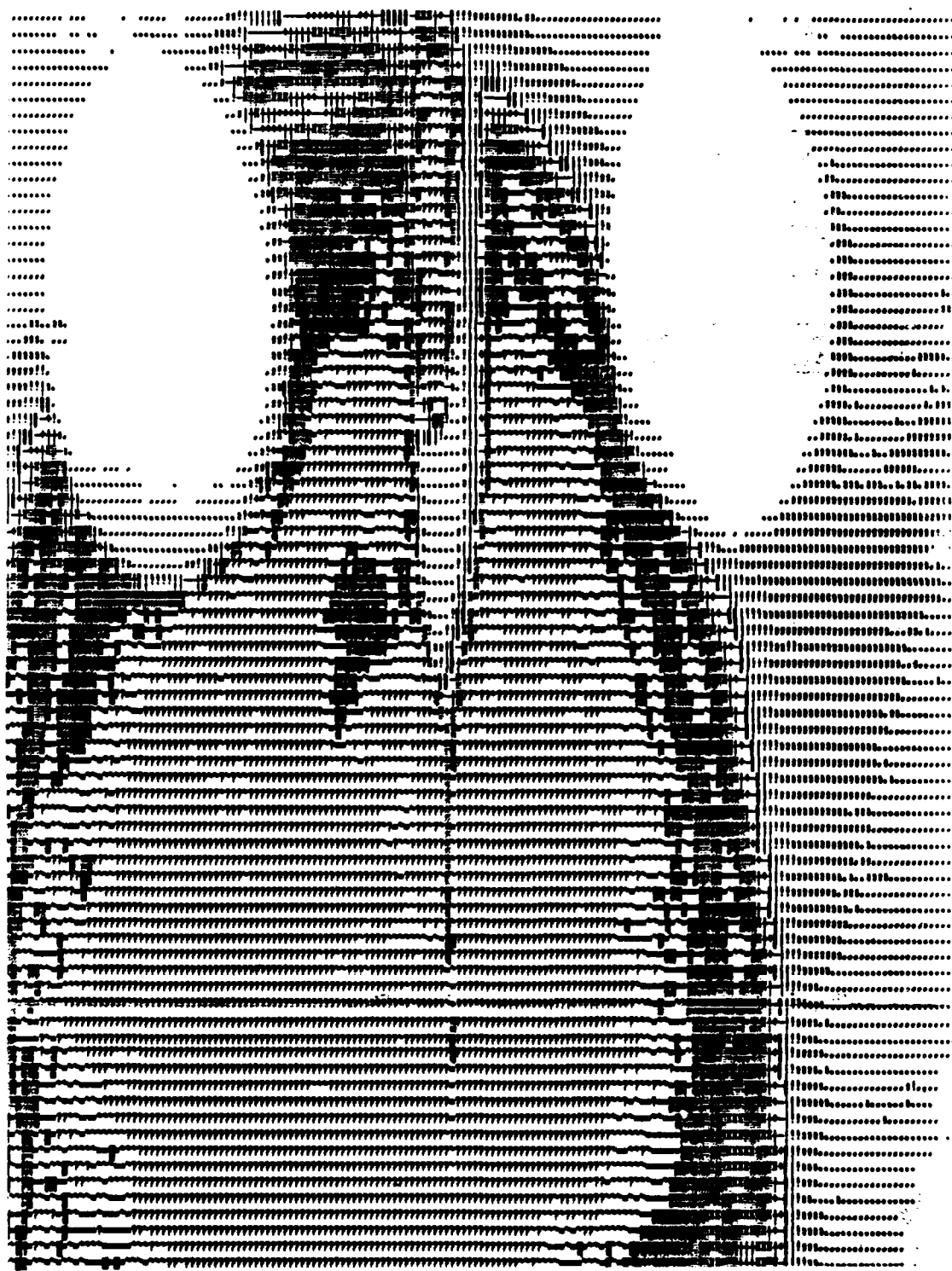
The digital images contained many artifacts but they were adequate to obtain precise crack measurements. We ascribe the artifacts to our lack of familiarity with the digitizing system used and insufficient shielding from stray light. The program budget did not permit the effort to remove the artifacts or rerun the data with better light masking.

Laser Experiment Data

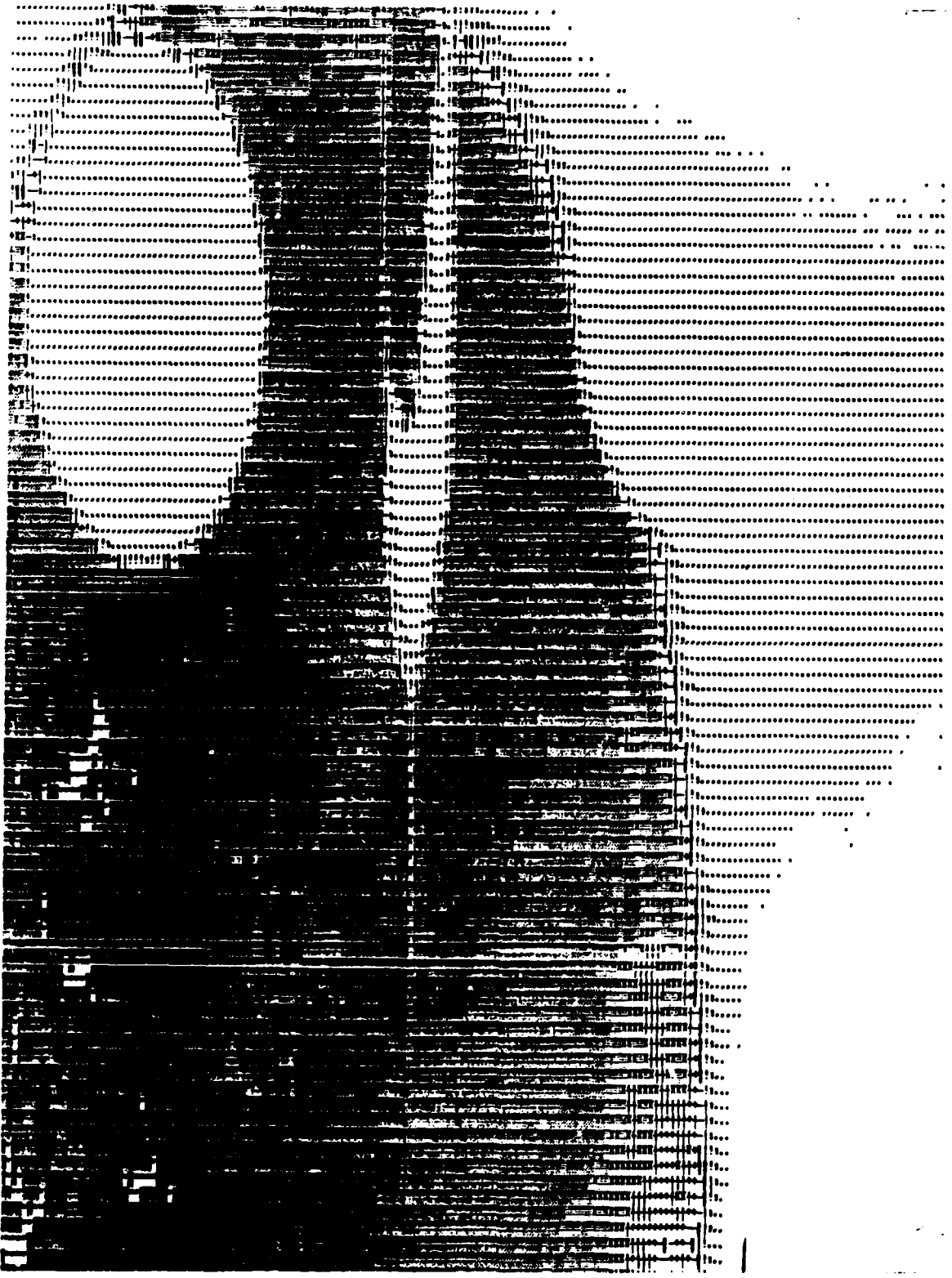
Film Number	2,000°F Temperature	Laser Illum.	Filter	Measure (in.)*	Error (%)
2	X			1.288	42.0
3	X			0.916	1.2
4	X	X		0.927	2.4
5	X	X	X	0.915	1.1
*Actual measurement 0.905 in. from end of crack to edge of specimen Specimen 304 SS provided by Foster-Miller					



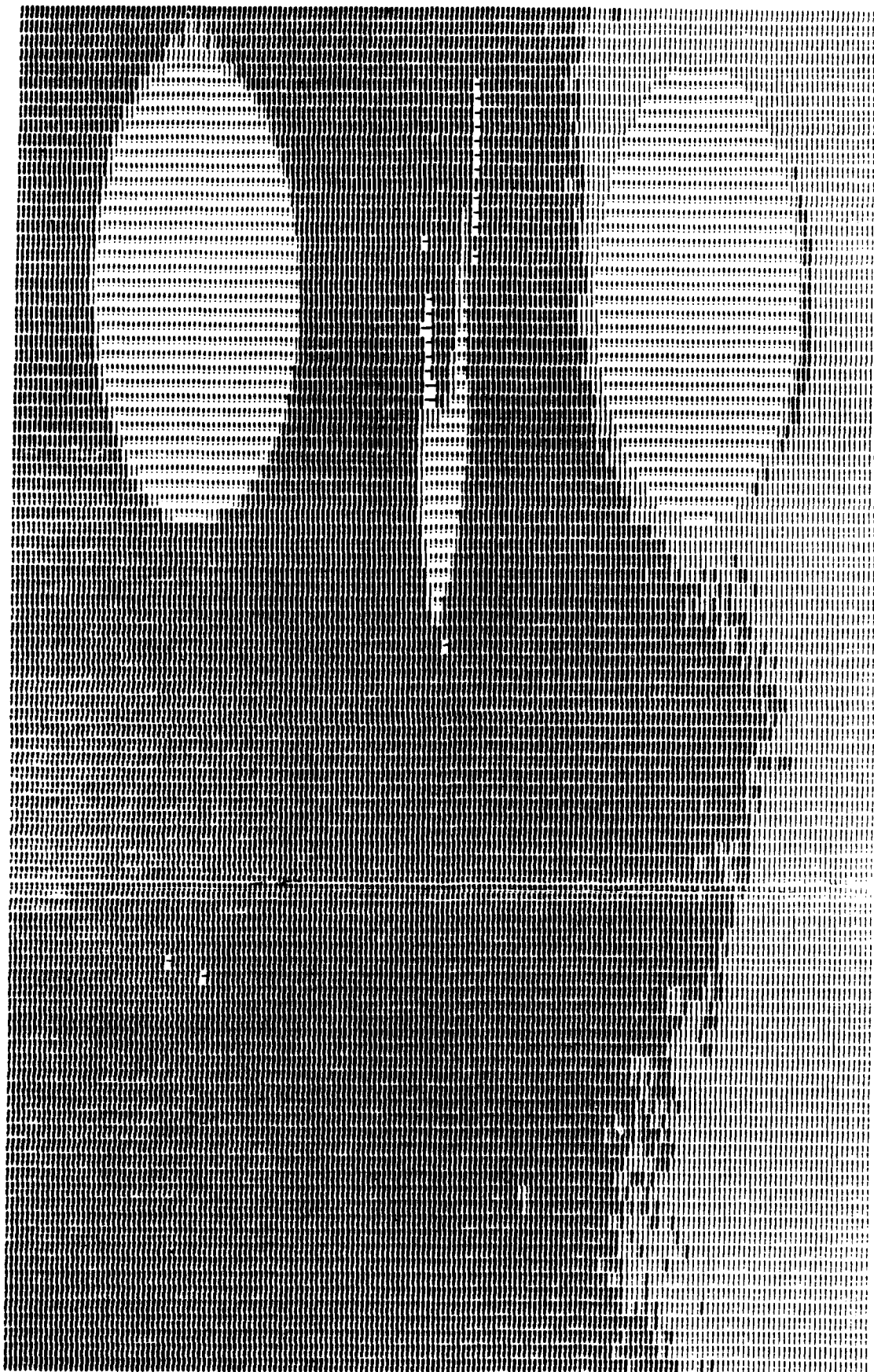
DIGITIZED LASER DATA
FILM 3



DIGITIZED LASER DATA
FILM 4



DIGITIZED LASER DATA
FILM 5



APPENDIX B

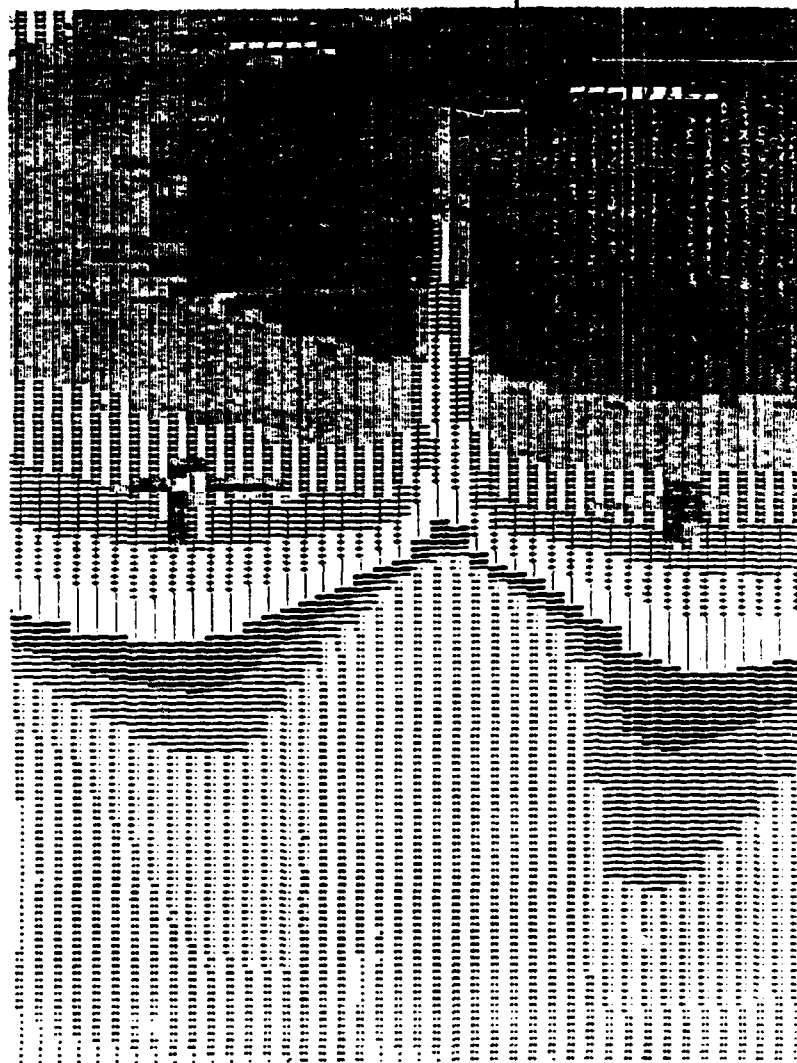
X-RAY EXPERIMENT DATA

The x-ray experiment data provided in Appendix B is summarized in the following table. The digital images that follow were generated directly from the photographic images presented in Section 4. Crack measurement was made by pixel counting from the crack tip to the edge of the specimen. Pixel calibration was accomplished by pixel counting the diameter of the specimen holes and comparing this count to the actual measurement of the hole diameter.

The digital images contained many artifacts but they were adequate to obtain precise crack measurements. We ascribe the artifacts to our lack of familiarity with the digitizing system used and insufficient shielding from stray light. The program budget did not permit the effort to remove the artifacts or rerun the data with better light masking.

Automatic Fatigue Crack Growth Measurement
X-Ray Experiment Data

Film Number	Angle of Incidence*	X-ray Dose Crack	(RADS) Surround	Measure (in.)**	Error (%)
1A	0	700	500	(3)	(3)
2	5	1100	500	0.809	0.9
3	10	700	600	0.636	21.0
4	20	500	400	0.619	23.0
5	30	500	400	***	***
<p>*Angle off perpendicular to specimen **Actual measurement 0.802 in. from end of crack to edge of specimen ***Lack of reference measurement voided data Specimen FF-3 provided by USAF</p>					

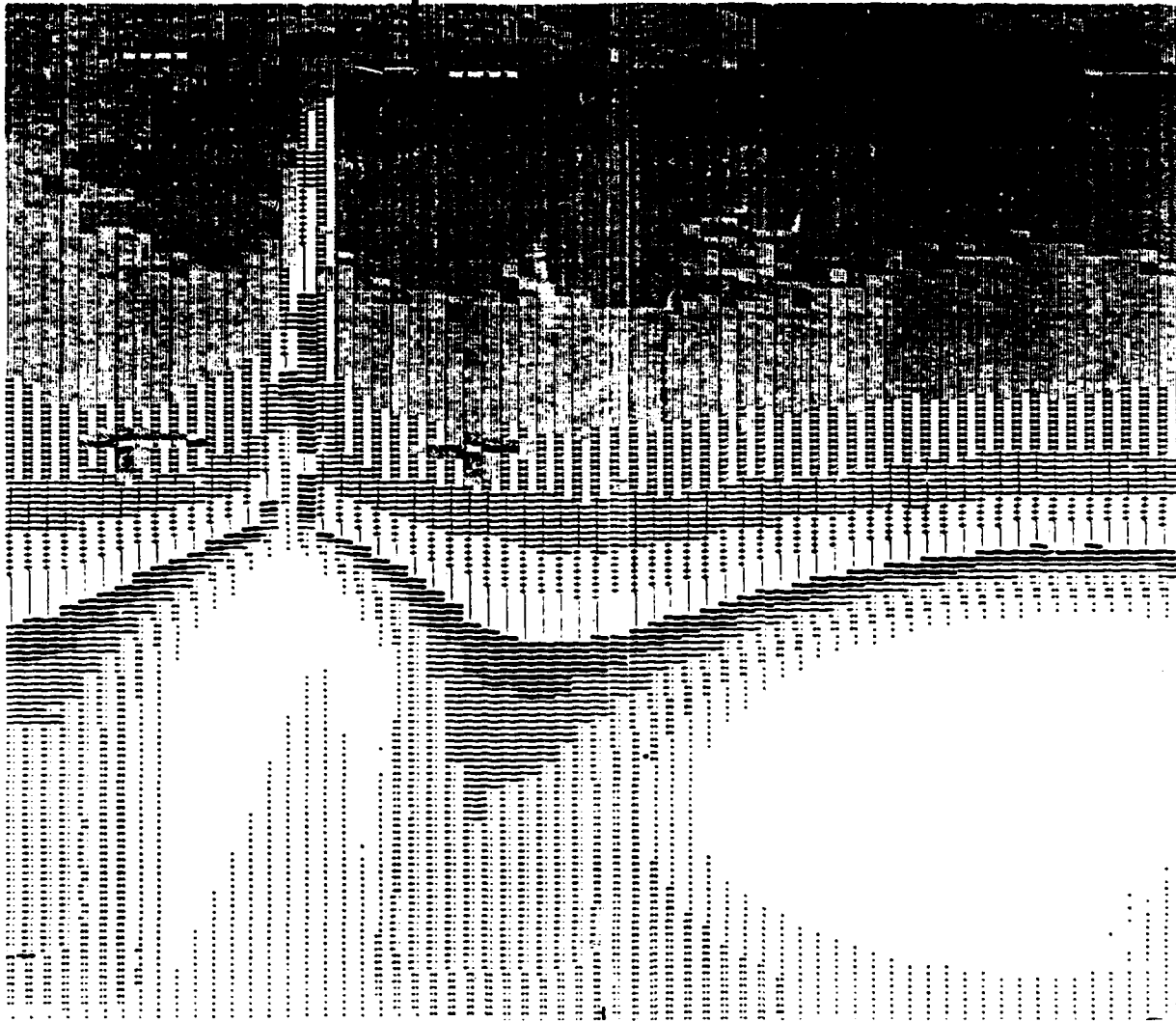


—CRACK TIP

DIGITIZED X-RAY DATA
FILM 1A



DIGITIZED X-RAY DATA
FILM 2



CRACK TIP

DIGITIZED X-RAY DATA
FILM 2 (WITH REFERENCE HOLE)

DATE
FILMED
— 8